European Journal of Medicinal Chemistry 214 (2021) 113219

Contents lists available at ScienceDirect

European Journal of Medicinal Chemistry

journal homepage: http://www.elsevier.com/locate/ejmech

Research paper

Design, synthesis, and biological evaluation of indazole derivatives as selective and potent FGFR4 inhibitors for the treatment of FGF19-driven hepatocellular cancer

Xiaolu Chen [a, 1], Yanan Liu [a, 1], Liting Zhang [a, 1], Daoxing Chen [a], Zhaojun Dong [a], Chengguang Zhao [a], Zhiguo Liu [a], Qinqin Xia [a], Jianzhang Wu [a, **], Yongheng Chen [b], Xiaohui Zheng [a, ***], Yuepiao Cai [a, *]

[a] School of Pharmaceutical Sciences, Wenzhou Medical University, Wenzhou, Zhejiang, 325035, China
[b] Department of Oncology, NHC Key Laboratory of Cancer Proteomics and Laboratory of Structural Biology, Key Laboratory of Medical Genetics and College of Life Science, and National Clinical Research Center for Geriatric Disorders, Xiangya Hospital, Central South University, Changsha, Hunan, 410008, China

ARTICLE INFO

Article history:
Received 1 October 2020
Received in revised form
15 January 2021
Accepted 17 January 2021
Available online 29 January 2021

Keywords:
Indazole derivatives
Hepatocellular carcinoma
Fibroblast growth factor receptor 4
Covalent inhibitor
Antitumor activity

ABSTRACT

Fibroblast growth factor receptor 4 (FGFR4) is a member of the fibroblast growth factor receptor family, which is closely related to the occurrence and development of hepatocellular carcinoma (HCC). In this article, a series of indazole derivatives were designed and synthesized by using computer-aided drug design (CADD) and structure-based design strategies, and then they were evaluated for their inhibition of FGFR4 kinase and antitumor activity. F-30 was subtly selective for FGFR4 compared to FGFR1; it affected cell growth and migration by inhibiting FGFR4 pathways in HCC cell lines in a dose-dependent manner.

1. Introduction

As high affinity receptors for fibroblast growth factors (FGFs), fibroblast growth factor receptors (FGFR1-4) are receptor tyrosine kinases (RTKS), which consist of an extracellular region, a transmembrane domain, and an intracellular tyrosine kinase region [1]. FGFR4 has been verified to play important roles in a variety of cell functions, such as cell proliferation, cell migration, differentiation, and biological processes, during the normal metabolic processes [2]. However, abnormal activation of the FGFR4 signaling pathway has been found to be closely associated with malignancy [3,4]. Aberrant activation of the FGFR4-FGF19 signaling pathway has been confirmed to be one of the carcinogenic factors in HCC. Human health is seriously threatened by the complexity and heterogeneity of HCC [5]. FGFR4 selectively binds FGF19 to stimulate autophosphorylation in trans and mediates cellular effects via downstream signaling pathways, which are involved in proliferation, anti-apoptosis, angiogenesis, drug resistance, invasion, and epithelial-to-mesenchymal transition in HCC cells [6]. Therefore, FGFR4 is considered an important target for the treatment of HCC. Small-molecule inhibitors targeting FGFR4 are a promising therapeutic approach for the treatment of HCC.

Great efforts have been made to develop effective FGFR4 inhibitors for anticancer treatment. Several multitargeting tyrosine kinase inhibitors (TKIs), such as ponatinib [7,8], dovitinib [9], lucitanib [10], have been studied for the suppression of FGFR4 signaling. Although these inhibitors have good kinase inhibitory activity against FGFR4, the toxicity profiles of those inhibitors relative to on-target activity against other kinases have restricted their further development for the treatment of HCC [11]. Non-covalent FGFR inhibitors, such as AZD4547 [12], NVP-BGJ398 [13], LY2874455 [14], and JNJ-42756493 [15,16], have been reported. Analysis of the ATP-binding domain of the FGFR kinase family has

* Corresponding author.
** Corresponding author.
*** Corresponding author.
E-mail addresses: wjzwzmu@163.com (J. Wu), zhengxh@wmu.edu.cn (X. Zheng), ypcai@wmu.edu.cn (Y. Cai).
[1] These authors contributed equally to this work.

https://doi.org/10.1016/j.ejmech.2021.113219
0223-5234/

found a unique cysteine for which it is possible to design covalent inhibitors on the P-loop ring. TAS-120 [17], FIIN-1 [18], FIIN-2 [19,20], FIIN-3 [20], FIIN-4 [21], and PRN1371 [22] were successively reported as FGFR covalent inhibitors (see Fig. 1). They function by introducing an acrylamide group to target Cys477. The acrylamide moiety undergoes a Michael addition reaction with the thiol group of cysteine to form a covalent bond. However, when these pan-inhibitors were used for treatment, patients had the severe toxic side effect of hyperphosphatemia due to on-target systemic inhibition of FGFR1 and FGFR3 [21]. Therefore, inhibitors selectively targeting FGFR4 may have better therapeutic effects with lower toxicity in HCC, and it is urgent to develop selective FGFR4 inhibitors.

Given the fact that the FGFR family proteins share significant sequence homology in their kinase domains, it has been a considerable challenge to develop inhibitors selective for FGFR4 over the other family members. In 2015, Hagel et al. reported a selective FGFR4 inhibitor, BLU9931, by targeting the conserved Cys552 in the hinge region of the FGFR4 protein sequence with an acrylamide moiety. An irreversible reaction of BLU9931 could occur with the sulfhydryl group of Cys552 by a Michael addition [23]. BLU9931 provided selective activity against FGFR4, which was more than 150-fold greater than its activity against FGFR1. Further optimization of BLU9931, with the aim of improving its physicochemical properties, afforded the clinical candidate BLU554 [5,24]. Disassembly and analysis of the quinoline scaffold was performed to obtain compounds 1 [25] and 2 [6,26] which had pyrimidine scaffolds. More recently, H3 Biomedicine developed the FGFR4-selective irreversible inhibitor H3B-6527, based on the structure of NVP-BGJ398, by adding an acrylamide moiety on the ortho position of the aniline group to target the Cys552 residue of FGFR4 [27]. The success of BLU9931 and H3B-6527 indicated that covalent modification based on pan-inhibitors was an effective tactic for designing FGFR4 inhibitors. Most recently, FGF401 was improved by Novartis as a highly-selective, reversible, covalent inhibitor of FGFR4 [28]. X-ray crystallography showed that a covalent bond was formed between the 2-formyl quinoline group and Cys552 by an addition reaction to generate a hemithioacetal adduct [29]. FGF401 displayed at least 1000-fold selectivity for FGFR4 over FGFR1/2/3 and other kinases. On account of its excellent antitumor activity and pharmacokinetics and pharmacodynamics, FGF401 has entered a phase I/II clinical trial to evaluate its safety and efficacy in HCC [30]. Although several inhibitors targeting FGFR4 have been reported, the chemical structural diversity of FGFR4 inhibitors still needs to be enriched. Therefore, our group used a compound-aided drug design strategy to analyze and explore the structure-activity relationship of reported FGFR4 inhibitors. We found an excellent combination of indazole scaffold with FGFR4 protein by studying the Protein Data Bank (PDB) reported structure. Then, a structure-based design strategy was used to explore the possibility of indazole derivatives as FGFR4 selective inhibitors. Herein, we report the design, synthesis, and evaluation of indazole derivatives as a novel class of potent, selective, and irreversible FGFR4 inhibitors.

2. Results and discussion

2.1. Design and SAR (structure-activity relationship) exploration

As shown in Fig. 2, a series of amino pyrazoles and their derivatives, which showed high FGFR kinase activities, have been reported.These include AZD4547, LY-2874455, 3 [31], 4 [32]. When we studied the reported pan-FGFR inhibitors, we discovered the significant role that aminopyrazole and aminoindazole scaffolds had played in designing FGFR inhibitors. Analyzing the binding pattern of the first reported aminopyrazole pan-FGFR inhibitor AZD4547 to FGFR4, we speculated that the aminopyrazole ring can be replaced with an aminoindazole ring [33]. Molecular docking was used to verify our conjecture. Compared to AZD4547, the benzamide portion of the new compound was closer to the hinge region. We wondered if the new compound could be designed as an FGFR4 inhibitor by introducing an acrylamide moiety.

As shown in Fig. 3B, the result of molecular docking showed that the acrylamide part could form a covalent bond with Cys552. The aminoindazole part could form two intramolecular hydrogen bonds with Ala553 and Glu551 on the hinge region. The 3,5-dimethoxyphenyl part extended to the hydrophobic pocket, which was in agreement with our design hypothesis. Hence, F-1 was synthesized (Fig. 3A). A kinase assay showed that the activity of

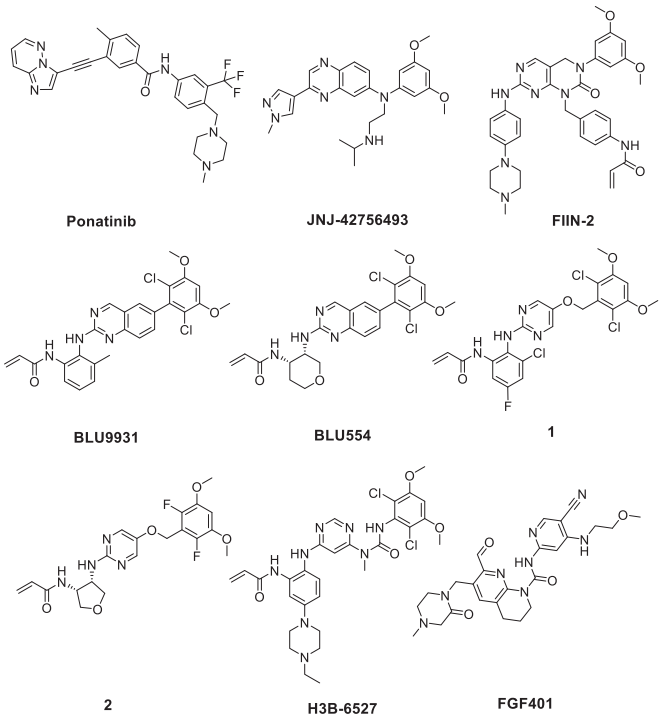

Fig. 1. Chemical structures of reported FGFR4 inhibitors.

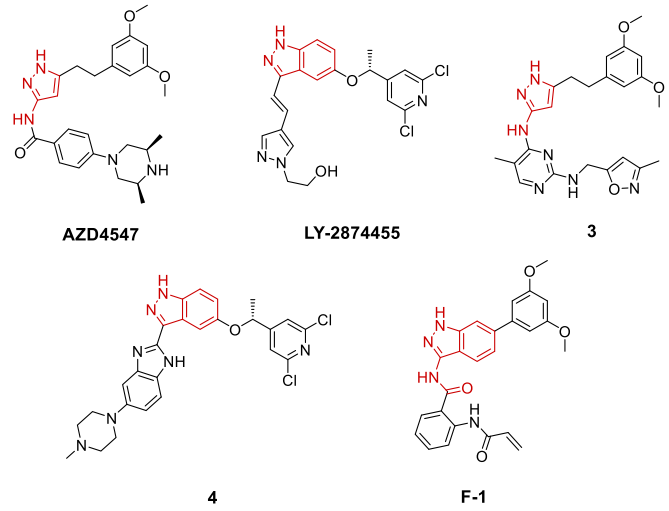

Fig. 2. Amino pyrazol Fibroblast Growth Factor Receptor (FGFR) Inhibitors.

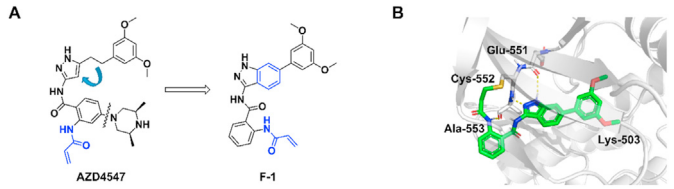

Fig. 3. (A) Design of our compound. (B) Covalent docking of compound F-1 with FGFR4 (PDB 4TYI).

the compound against FGFR4 was observable at 160 nM. This activity was more than 10-fold greater than its activity against FGFR1. This revealed the potential of compound F-1 to be an FGFR4 inhibitor. Therefore, F-1 was taken as the lead compound for further optimization.

2.2. Chemistry

The designed inhibitors were readily prepared by a Suzuki coupling as the key step (Scheme 1). Briefly, reaction of the commercially available 4-bromo-2-fluorobenzonitrile with hydrazine hydrate produced intermediate 5, and then commercially available di-tert-butyl pyrocarbonate reacted with intermediate 5 in the presence of 4-dimethylaminopyridine (DMAP) to provide the intermediate 6. Next, 7a–7b were obtained by a nucleophilic substitution reaction between intermediate 6 and ortho or meta-position nitro-substituted benzoyl chloride. Compounds 7a–7b were coupled with various substituted boronic acids or boronic acid esters to afford the Suzuki-coupling product 8. The catalytic hydrogenation of the nitro-group with Pd/C provided the desired aniline 9 in high yield. Intermediate 9 was reacted with different acyl chlorides and deprotected to produce the designed molecule 10 with good yields. The other designed inhibitors were synthesized by utilizing a similar protocol (Scheme S1).

Reagents and conditions:(a) hydrazine hydrate, 2-amyl alcohol, 120 °C, 3 h, 81%–95%; (b) $(Boc)_2O$, DMAP, THF, rt, 0.5 h, 77%–84%; (c) 2-nitro-benzoyl chloride or 3-nitro-benzoyl chloride, DIPEA, 1,4-dioxane, 0 °C to rt, 68%–89%; (d) Pd $(pph_3)_4$, Cs_2CO_3, boronic acid/ester, 1,4-dioxane, 120 °C, 1 h, 60%–82%; (e) Pd/C, H_2, CH_3OH, overnight, 70%–92%; (f) substituted acetyl chloride, DIPEA, 1,4-dioxane, 0 °C to rt, 2 h, 66%–78%; (g) TFA, DCM, rt, 3 h, 45%–56%.

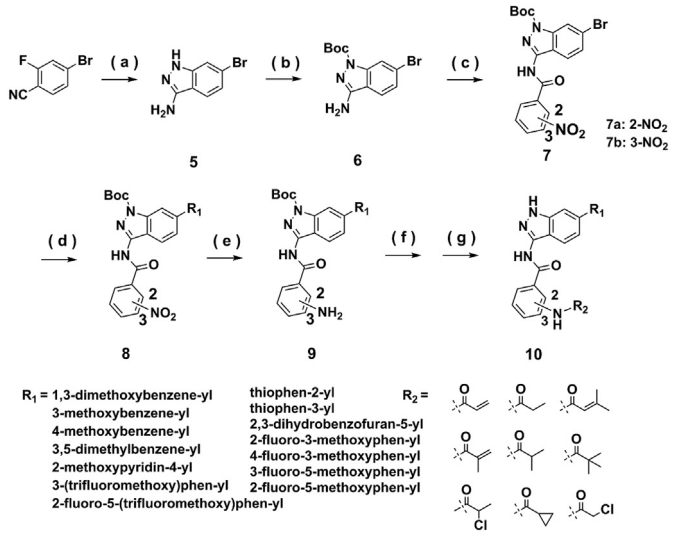

Scheme 1. Synthesis of Compounds F-1—F-14, F-20—F-33 and F1-1—F1-2.

The binding mode of the lead compound F-1 predicted that the 3, 5-dimethoxyphenyl was adjacent to the gatekeeper Asp630. For initial structure-activity relationship exploration, we assumed that modification of this position might bring about a good effect on the selectivity of compounds. Therefore, a series of compounds with a ring substituent of R_1 were studied. When the 3, 5-dimethoxyphenyl was replaced by 3-methoxyphenyl (F-2), the potency against FGFR4 decreased a little. However, changing of the substituent group of 3-methoxyl to 4-methoxyl (F-3) and 3, 5-dimethylphenyl (F-4) led to a 3-fold decrease of potency against FGFR4. Introducing a trifluoromethoxy (F-9, F-10) almost abolished the FGFR4 activities of the compound. After substitution of the benzene ring with a pyridine ring (F-5), benzofuran (F-8) and thiophene (F-6, F-7) showed decreased inhibitory activity against FGFR4. Previous data indicate that the introduction of a fluorine atom in the benzene ring can improve potency. In drug development, researchers found the fluorine atom had the dual property of hydrogen bond acceptor and hydrophobic moiety [34]. Therefore, compounds F-11, F-12, F-13, and F-14 were synthesized. Surprisingly, F-11 and F-14 had higher IC_{50} and selectivity than F-1. And then, the focus of previous studies had been transferred to the N-substituted indazole ring, to explore the potency of different scaffolds. Therefore, compounds F-15—F-19 were synthesized by utilizing a similar protocol (Scheme S1). Kinase inhibitory activity suggested that the indazole ring was suitable for further exploration (see Table 1).

Because compound F-1 had higher potential for inhibiting FGFR4 than FGFR1, there was an assumption that an acrylamide moiety could target the Cys552 residue, which was crucial to the design of FGFR4 inhibitors. In order to improve the potency of FGFR4 further, we investigated this. Compounds F-20—F-27, with different “warheads” adjacent to acid amides, were synthesized. Surprisingly, none of these compounds showed good IC_{50} value (see Table 2). It is likely that the length of the warheads and steric hindrance contributed to this result. We asked what conformation would be seen if the warhead was put in the meta-position of the acid amides. Surprisingly, compound F-30, with a halogen warhead, showed good FGFR4 kinase activity with an IC_{50} value of 8.6 nM as well as remarkable selectivity against FGFR1.

Combining the best fragments above, F-30, F1-1, and F1-2 were synthesized for the purpose of obtaining FGFR4 inhibitors with better kinase activity and selectivity. As shown in Table 3, all three compounds showed excellent FGFR4 kinase activity. Unexpectedly, F-30, F1-1, F1-2 also showed good potency against FGFR2 and FGFR3, but they had less inhibition effect on FGFR1. Thus, compounds F-30 and F1-2 were chosen as representatives for further investigation due to their strong FGFR4 inhibitory potency and good selectivity against FGFR1.

2.3. F-30 blocking FGFR4 signaling in HCC cells

The Cancer Genome Atlas (TCGA) is a large cancer genomics program, molecularly characterizing over 20,000 primary cancers and matched normal samples spanning 33 cancer types [35]. Exploring from the TCGA datasets, we validated that liver hepatocellular carcinoma (LIHC) patients in the TCGA database express much higher mRNA in tumor tissue than in normal tissue (Fig. 4A). In addition, patients expressing higher FGFR4 showed lower survival rates compared to patients with low FGFR4 expression (Fig. 4B).

Therefore, we selected hepatocellular carcinoma cell lines to validate further the FGFR4 inhibition effect of compound F-30. Western blot analysis was performed to determine which related signaling pathway was involved in HUH7, HepG2, and SMMC-7721 cell lines (Fig. 4C, 4D, 4E, and S1). Compound F-30 inhibited

Table 1
Structure-activity relationships in the modification of hydrophobic Region.

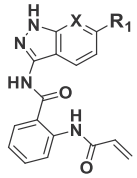

Compounds	X	R1	Kinase inhibitor activity (IC_{50}, nM)	
			FGFR1	FGFR4
F-1	C		>1500	120
F-2	C		>1500	273
F-3	C		>1500	423
F-4	C		>1500	632
F-5	C		>1500	>1500
F-6	C		>1500	258
F-7	C		>1500	>1500
F-8	C		>1500	>1500
F-9	C		>1500	1137
F-10	C		>1500	>1500
F-11	C		>1500	60
F-12	C		>1500	>1500
F-13	C		>1500	304
F-14	C		>1500	100
F-15	N		>1500	449
F-16	N		>1500	726
F-17	N		>1500	374
F-18	N		>1500	>1500
F-19	N		>1500	446

Table 2
Structure-activity relationships in the modifications of Warheads.

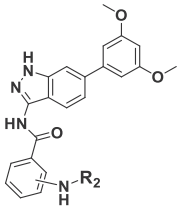

Compounds	o/m[a]	R_2	Kinase inhibitor activity (IC_{50}, nM)	
			FGFR1	FGFR4
F-1	o		>1500	160
F-20	o		>1500	>1500
F-21	o		>1500	>1500
F-22	o		>1500	>1500
F-23	o		>1500	>1500
F-24	o		>1500	>1500
F-25	o		>1500	>1500
F-26	o		>1500	>1500
F-27	o		>1500	>1500
F-28	m		>1500	>1500
F-29	m		>1500	>1500
F-30	m		>1500	8.6
F-31	m		>1500	>1500
F-32	m		>1500	>1500
F-33	m		>1500	>1500

[a] "o": ortho-substituted of the benzamide; "m": meta-substituted of the benzamide (see Table 2).

FGF19-induced FGFR4 phosphorylation and the phosphorylation of downstream kinases MAPK in a concentration-dependent manner, while the total amounts of their target proteins remain unchanged. The MAPKs are abnormally expressed in a series of cancers and are involved in the regulation of cell proliferation, migration, survival, and apoptosis [36]. Phosphorylation of FGFR4 and MAPK was almost undetectable in HUH7 cells treated with 0.625 μM of compound F-30. Together, these results confirmed that F-30 could block the FGFR4 signaling pathway by inhibiting the phosphorylation of FGFR4.

2.4. F-30 inhibits cell invasion in HCC

FGFR4-dependent signaling pathways involve cell invasion, migration, and proliferation [37]. We observed obvious morphological changes of F-30-treated HCC cells. Therefore, we speculate that F-30 might affect the expression and function of cytoskeletal proteins of HUH7 cells. Focal adhesion kinase (FAK) is a non-receptor tyrosine kinase that regulates adhesion spot integrity, which plays an important role in maintaining cell morphology, cell division, cell mobility, and other activities which play an important role in tumorigenesis [38]. To explore whether F-30 treatment

Table 3
Structure-activity relationships in the modification of hydrophobic region and warhead.

Compounds	R_1	R_2	Kinase inhibitor activity (IC_{50}, nM)			
			FGFR1	FGFR2	FGFR3	FGFR4
F-30			>1500	15	146	8.6
F1-1			106	15	86	5.6
F1-2			528	27	208	6.8
BLU9931	—	—	—	—	—	6.3
staurosporine	—	—	21	7.4	16	240

affected the expression and distribution of FAK, an immunofluorescence (IF) assay was performed using *anti*-FAK antibody. The results indicated that the area of fluorescence decreases and the intensity of fluorescence weakens at different concentrations (Fig. 5A and 5B). Additionally, Western blot assay showed that F-30 inhibited the expression of *p*-FAK and FAK in HUH7 cell lines in a concentration-dependent manner (Fig. 5C).

Adhesion of metastatic cancer cells to the vascular endothelium of the target organs is the key occurrence in transendothelial migration [39]. In this study, an adhesion assay was performed to test whether F-30 could reduce cell adhesion. As shown in Fig. 5D, F-30 significantly reduced the adhesion ability of the HUH7 cell lines compared to the control. There was a dose-effect relationship between the adhesion rate and F-30, and the adhesion rate of 5.0 μM F-30 treated cells was only 50% of that of the control. Similar results were obtained in HepG2 and SMMC-7721 cells. (Figure S2. A). Furthermore, transwell invasion assays were used to explore the effect of F-30 on the invasion ability of HCC cells. Compared to control, F-30 at different concentrations (0, 1.25, 2.5, and 5 μM) significantly inhibited the invasion of HUH7 (Fig. 5E) and SMMC-7721 (Figure S2·B) cells. The wound healing assay indicated that different concentrations of F-30 markedly inhibited migration of HUH7 (Fig. 5F and 5G) and SMMC-721 cell lines (Figure S2·C).

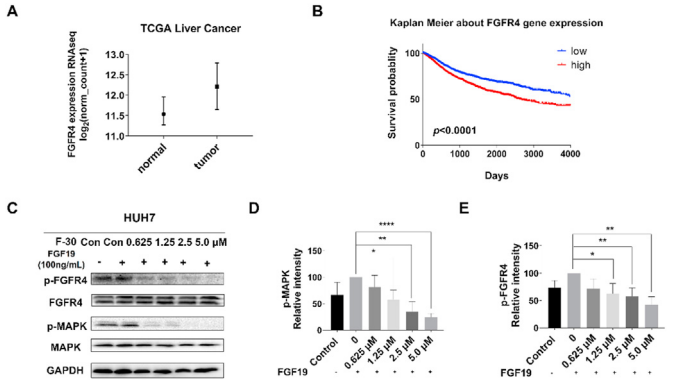

Fig. 4. F-30 inhibited the phosphorylation of FGFR4 and its downstream pathways. (A) Plots were based on the expression values of FGFR4 in liver cancer samples compared to normal tissues (n = 423). (B) Kaplan–Meier analysis showed the association between FGFR4 expression and disease-free survival or overall survival of liver cancer patients. Data was acquired from The Cancer Genome Atlas (TCGA). (C) Compound F-30 dose-dependently inhibited the activation of FGFR4 and downstream proteins in HUH7 cells. HUH7 were incubated with the F-30 at different concentrations for 6 h and then added FGF19 before cell lysis. Western blot analysis was used to determine the protein expression of *p*-FGFR, FGFR4, *p*-MAPK, MAPK. GAPDH was used as loading control. The results were representative of three replicated experiments. (D), (E) The intensity of *p*-FGFR4 and *p*-MAPK were calculated.

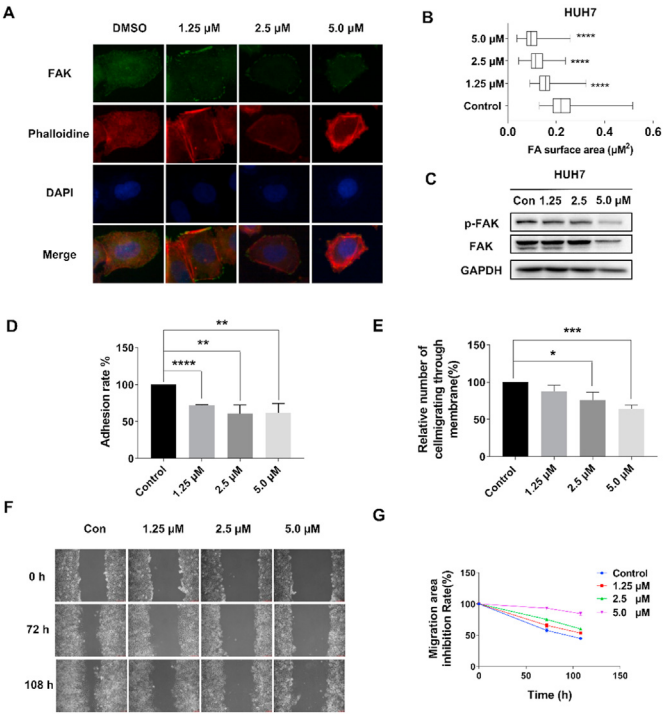

Fig. 5. F-30 induced cancer cell migration. (A), (B) Cells were incubated with the F-30 at different concentrations for 12 h. The expression of FAK (green) in HUH7 cells was determined by immunofluorescence assay. Phalloidine-stained actin red, DAPI-stained nuclei blue. The area of FAK surface was calculated. (C) Western-blot assay was performed to analysis phosphorylation and total FAK levels in HUH7 treated with F-30 in different concentration. (D) Cell adhesion assay and invasion assay was performed to evaluate the migration impact of F-30 on HUH7. The results were representative of three replicate experiments. (E) HUH7 cells were treated with F-30 at different concentrations for 12 h. The migratory capacity of cells was then assessed. (F) Wound healing assays examined the effects of F-30 on HUH7 cell migration, and migration area was calculated (G).

2.5. F-30 inhibits HCC cells proliferation

To explore the antitumor activity of F-30 further, an MTT assay was carried out. The quantitative data demonstrated that F-30 efficiently decreases the viability of HCC cells in a concentration-dependent manner, with an IC_{50} of 3–5 μM. Compared to the positive control BLU9931, a potent, selective, and irreversible FGFR4 inhibitor, F-30 was more cytotoxic to HCC cells (Fig. 6A, 6B, 6C). Furthermore, F-30 significantly reduced colony formation of three HCC cell lines in a dose-dependent manner (Fig. 6D).

Next, we treated the three human HCC cell lines with F-30 at different concentrations (0, 1.25, 2.5, and 5.0 μM) for 48 h, and then observed apoptosis by flow cytometry (FCM). Treatment with F-30 increased the proportion of apoptotic cells in a dose-dependent manner (Fig. 6E and 6F, and S3·B). Similar apoptotic effects were shown by morphological changes in cell nuclei by Hoechst staining. Overall, these results suggested that F-30 significantly inhibits cell survival and increases apoptosis in HCC cells (Fig. 6G).

Further studies were carried out to see how F-30 induces apoptosis. Genomic stability relies on an effective DNA damage repair pathway to retain the chromosomes intact [40]. Introducing DNA damage not only causes genome mutations but also accumulates cell cycle arrest and finally apoptosis. We hypothesized that apoptosis might be caused by F-30 induced DNA damage. To confirm this hypothesis, we performed an immunofluorescence assay with antibody against p53-binding protein 1 (53BP1), an important regulator in the response to DNA damage. The amount of

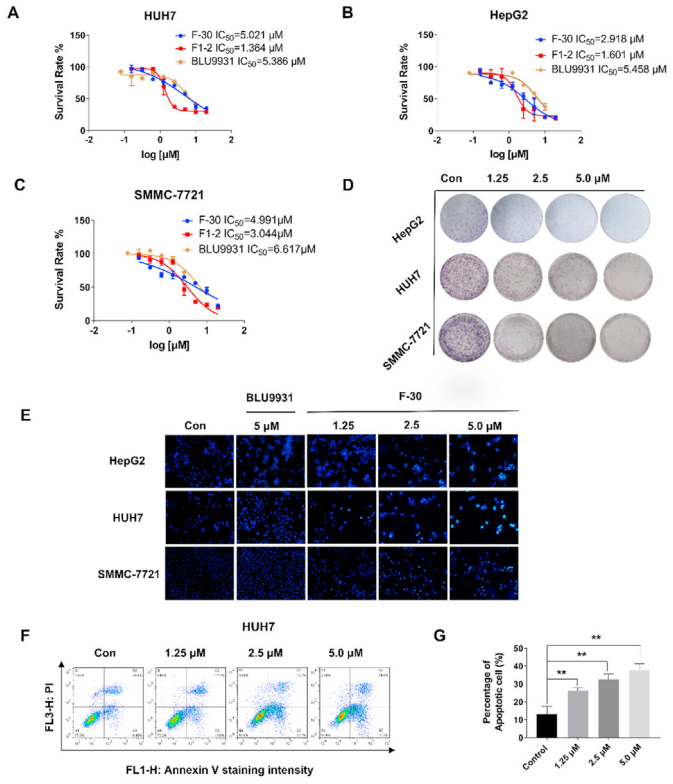

Fig. 6. F-30 showed promising efficacy to suppress HCC cells proliferation. (A) IC_{50} values of F-30 in HCC. Three HCC lines were seeded in 96-well plates and treated with various concentrations of F-30. Proliferation was measured after 48 h of treatment by the MTT assay. Data were expressed as the mean ± SD of 3 independent experiments. (B) Colony-forming assay of the indicated cell lines. The cell was incubated with F-30 for 24 h. On day 7, colonies were fixed and photographed. Representative images were displayed. (C) HUH7 cells were treated with the indicated concentrations of F-30 and incubated for 48 h. Cells were stained with Annexin V and propidium iodide (PI) and then analyzed by flow cytometry. (E) Cell stained with Hoechst staining was observed in HUH7, HepG2, and SMMC-7721 with F-30 for 12 h.

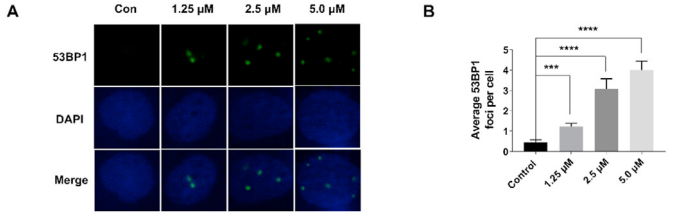

Fig. 7. F-30 induced tumor cell apotosis. (A) HUH7 cells were incubated with the F-30 at different concentrations for 12 h 53BP1 (green) immunofluorescence assay was performed, DAPI-stained nuclei blue. (B) Green focis were counted to make statistics.

53BP1 represents the level of DNA damage. As shown in Fig. 7A and 7B, with increasing concentrations of drug, increasing numbers of 53BP1 foci gathered in the nuclei in HUH7 cell lines. In the untreated group, there were almost no foci, but the average number of foci per cell at the highest concentration was six times higher than in the control group. F-30 showed the same effect in the SMMC-7721 cell line (Figure S3. A).

2.6. Molecular docking of compound F-30 to FGFR4

To investigate the binding mode of the inhibitor we had designed, F-30 was docked into the ATP-binding pocket of FGFR4 (PDB: 4TYI). As portrayed in Fig. 8A, the 1*H*-indazol-3-amine

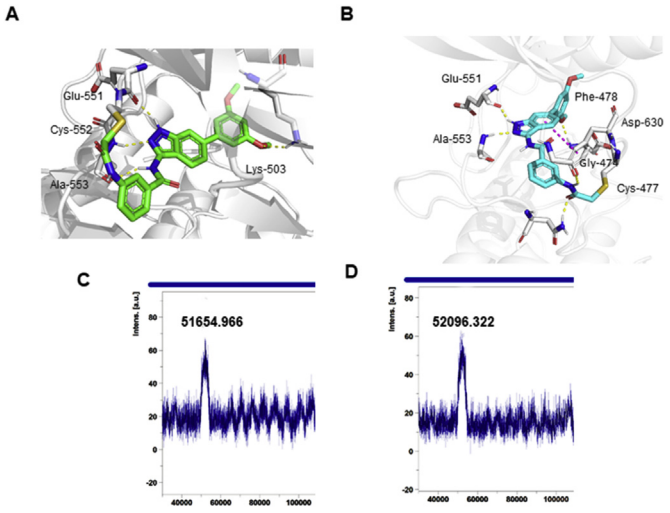

Fig. 8. (A) Predicted binding model of F-30 and FGFR4 (PDB 4TYI). (B) Predicted binding model of F-30 and FGFR4 (PDB 5NWZ). (C) MALDI-TOF MS determination of FGFR4. (D) MALDI-TOF MS determination of FGFR4 and FGFR4/F-30 complex.

scaffold was adjacent to the hinge region of the FGFR4 protein and interacted effectively with Glu551 and Ala553 through three H bonds. The 3, 5-dimethoxybenzene motif was anchored to the hydrophobic region by adopting the parallel orientation with respect to the plane of the 1*H*-indazol-3-amine core; an H bond was present between the oxygen atom of the 3-methoxy and the amine of Lys 503. Benzamide-linked 2-acetbromamide was poised in a suitable position to engage Cys552 in a covalent bond. This reasonable combination mode indicates a rational design of our inhibitor, which convinced us of our design approach. To discover more possible binding modes, we docked F-30 with another FGFR4 protein (PDB 5NWZ). What we found interesting was that F-30 also covalently bound to Cys477. The 1*H*-indazol-3-amine scaffold interacted effectively with Glu551 and Ala553 and formed two H bonds. The 3, 5-dimethoxybenzene motif vertically inserted into the hydrophobic pocket and form H bond with the residue of Asp630 (Fig. 8B). Combining the kinase activities of F-30, F1-1, F1-2, and the selectivity theory of FGFR4 inhibitors reported by Lin's group [41], we predicated that F-30 was covalently bound to Cys477/Cys 522 which lead to the selectivity against FGFR1. On account of the high homologous of FGFR1-4 kinase sequence, the p-loop cysteine is conserved across FGFR1-4. Hence, the covalent binding mode of the p-loop cysteine of FGFR4 could occur to a greater or lesser extent across the FGFR1/2/3. It means that F-30 may covalently bind to the cysteine on the p-loop ring of FGFR1/2/3 protein and eventually lead to the different selectivity against FGFR1/2/3.

2.7. F-30 covalently binds to FGFR4 protein

To verify whether compound F-30 inhibited FGFR4 kinase via irreversible binding, MALDI-TOF MS assay was performed to confirm the covalent binding. In this assay, FGFR4 kinase was preincubated with compound F-30 at 4 °C for 24 h. As shown in Fig. 8C and 8D, the molecular weight of FGFR4 was 51,654.966 Da, and the molecular weight of FGFR4 incubated with F-30 was 52,096.322 Da, consistent with the sum of the molecular weights of the kinase and compound within the margin of error. This assay suggested that F-30 could irreversibly bind to FGFR4.

3. Conclusion

Uniting the structure-based design and computer-aided drug design strategies, a series of indazole derivatives were designed and synthesized as novel potent FGFR4 inhibitors. After three rounds of structure-activity relationship exploration, kinase activities indicated that compounds F-30, F1-1, and F1-2 had better inhibitory activity to FGFR4 kinase with different FGFR1 selectivity. It was found that F-30 and F1-2 showed excellent FGFR4 selectivity against FGFR1, compound F-30 had the best selectivity against FGFR1. Moreover, all three compounds showed better antitumor activity than BLU9931 in a dose-dependent manner in three FGFR4 high-expression HCC cell lines. In addition, F-30 exhibited a potent antiproliferative effect against FGFR4 high-expression HCC cell lines HUH7, HepG2, and SMMC-7721 through potent inhibition of the MAPK signaling pathways, suppression of cell cycle progression, and induction of apoptosis. Further study confirmed that apoptosis was induced by DNA damage. Additionally, F-30 inhibited the expression of *p*-FAK and FAK, adhesion, and invasion ability of HCC cell lines in a dose-dependent manner. Mass spectrometry experiments showed that F-30 was bound to FGFR4 protein via covalent combination manner. The expected aim to design covalent inhibitor has been achieved. Although we expected the compounds to target the hinge Cys552 of FGFR4 at the beginning of the experiment, molecular docking of compound F-30 with FGFR4 protein suggested that F-30 could bind to Cys552 or Cys477. Considering that the cysteine of the p-loop ring is conservatively present in FGFR1-4, we suspected that the preferred compound F-30 could bind to the cysteine of the p-loop ring of FGFR1/2/3 covalently to different extent. That may explain the difference in biochemical IC_{50} for the F-30 across FGFR1/2/3. A deep mechanism of the binding model is underway, and we will give it further exploration. Altogether, this target compound showed promise for more exploration as a selective FGFR4 inhibitor for the treatment of HCC. Further studies on structural optimization and biological activities of these derivatives are still in progress in our laboratory. And we are supposed to find highly effective FGFR4 inhibitors in the future.

4. Experimental section

4.1. Chemistry

All starting materials and regents were acquired from commercial suppliers or prepared according to known procedures. All starting materials and solvents were used without further purification. Chemical reactions were monitored by thin-layer chromatography (TLC), using silica gel plates with fluorescence F254 and visualized under UV light. Flash chromatography was conducted using silica gel (200−300 mesh). ^{1}H NMR and ^{13}C NMR were generated in DMSO-d_6 on Bruker 400 or 500 NMR spectrometers. All tested compounds were purified to ≥95% purity by the Agilent infinity 1260 HPLC system.

4.2. General procedure for synthesis of compounds (take F-1 as example)

6-bromo-1*H*-indazol-3-amine (5). To a solution of 4-bromo-2-fluorobenzonitrile (1 eq, 100 mg) in 2-amyl alcohol (4 mL) was added hydrazine hydrate (5 eq, 125 mg), the mixture was stirred at 120 °C for 3 h. Then the solution was cooled to the room temperature, filtered and washed by ethyl alcohol to give the title compound 5 as white crystalline solid (86 mg, 81%). ^{1}H NMR (400 MHz, DMSO-d_6) δ 11.51 (s, 1H), 7.66 (d, J = 8.5 Hz, 1H), 7.46 (d, J = 0.9 Hz, 1H), 7.02 (dd, J = 8.5, 1.3 Hz, 1H), 5.48 (s, 2H).

Tert-butyl 3-amino-6-bromo-1*H*-indazole-1-carboxylate (6). To a mixture of compound 5 (1 eq, 5 g), DMAP (0.2 eq, 435 mg), THF (50 mL) was added $(Boc)_2O$ (1.2 eq, 6.175 g) dropwise, the solution was stirred at room temperature for 0.5 h. Then the solution was concentrated with a rotary evaporator, the mixture was poured into water and extracted with CH_2Cl_2 (3 × 15 mL). The organic layer was washed with saturated aqueous NaCl, dried over anhydrous Na_2SO_4, concentrated in vacuo, purified by silica gel chromatography (petroleum ether/ethyl acetate/dichloromethane = 4:1:1, v/v/v) to give the product 6 as a white solid (6.183 g, 84%). ^{1}H NMR (400 MHz, DMSO-d_6) δ 8.11 (s, 1H), 7.80 (d, J = 8.4 Hz, 1H), 7.44 (dd, J = 8.4, 1.5 Hz, 1H), 6.42 (s, 2H), 1.57 (s, 9H).

Tert-butyl 6-bromo-3-(2-nitrobenzamido)-1*H*-indazole-1-carboxylate (7). To a solution of compound 6 (1 eq, 100 mg) in 1, 4-dioxane (20 mL) was added acryloyl chloride (2.5 eq, 149 mg) dissolved in DCM (0.5 mL) at 0 °C. The reaction solution was stirred at room temperature for 3 h. The mixture was poured into water and extracted with CH_2Cl_2 (3 × 20 mL). The organic layer was washed with saturated aqueous NaCl, dried over anhydrous Na_2SO_4, and concentrated in vacuo. The residue was purified by silica gel chromatography (petroleum ether/ethyl acetate/dichloromethane = 3:1:1, v/v/v) to give the title product 7 as a white solid (126 mg, 85%). ^{1}H NMR (400 MHz, DMSO-d_6) δ 11.78 (s, 1H), 8.29 (s, 1H), 8.18 (d, J = 8.1 Hz, 1H), 7.99 (d, J = 8.7 Hz, 1H), 7.88 (d, J = 6.9 Hz, 2H), 7.78 (t, J = 7.1 Hz, 1H), 7.59 (dd, J = 8.7, 1.4 Hz, 1H), 1.63 (s, 9H).

Tert-butyl 6-(3,5-dimethoxyphenyl)-3-(2-nitrobenzamido)-1*H*-indazole-1-carboxylate (8). To a mixture of compound 7 (1 eq, 400 mg), Cs_2CO_3 (2 eq, 566 mg), (3, 5-dimethoxyphenyl)boronic acid (2 eq, 316 mg) in 1,4-dioxane (20 mL) was added Pd $(pph_3)_4$ (0.1 eq, 100 mg), the solution was stirred at 110 °C under N_2 atmosphere for 1 h. Then the solution was concentrated with a rotary evaporator. The mixture was poured into water and extracted with CH_2Cl_2 (3 × 15 mL). The organic layer was washed with saturated aqueous NaCl, dried over anhydrous Na_2SO_4, and concentrated in vacuo. The residue was purified by silica gel chromatography (petroleum ether/ethyl acetate/dichloromethane = 2:1:1, v/v/v) to give the product 8 as a white solid (400 mg, 77%). ^{1}H NMR (400 MHz, DMSO-d_6) δ 11.72 (s, 1H), 11.72 (s, 1H), 11.72 (s, 1H), 8.31 (s, 1H), 8.31 (s, 1H), 8.31 (s, 1H), 8.18 (t, J = 10.2 Hz, 1H), 8.09 (d, J = 8.5 Hz, 1H), 7.89 (s, 2H), 7.80 (d, J = 8.1 Hz, 1H), 7.73 (d, J = 8.5 Hz, 1H), 6.87 (d, J = 1.3 Hz, 2H), 6.58 (s, 1H), 3.83 (s, 6H), 1.66 (s, 9H).

Tert-butyl 3-(2-aminobenzamido)-6-(3,5-dimethoxyphenyl)-1*H*-indazole-1-carboxylate (9). To a solution of compound 8 (400 mg) in CH_3OH (15 mL) was added catalytic Pd/C, then the reaction was stirred overnight in hydrogen environment. Then the mixture was filted and the filtrate was concentrated with a rotary evaporator. The residue was purified by silica gel chromatography (petroleum ether/ethyl acetate/dichloromethane = 5:1:1, v/v/v) to give the product 9 as a white amorphous solid (343 mg, 91%). ^{1}H NMR (500 MHz, DMSO-d_6) δ 11.00 (s, 1H), 8.30 (s, 1H), 7.94−7.75 (m, 2H), 7.66 (d, J = 8.5 Hz, 1H), 7.24 (t, J = 7.6 Hz, 1H), 6.86 (s, 2H), 6.78 (d, J = 8.3 Hz, 1H), 6.62 (s, 2H), 6.57 (t, J = 7.4 Hz, 2H), 3.82 (s, 6H), 1.67 (s, 9H).

Tert-butyl 3-(2-acrylamidobenzamido)-6-(3,5-dimethoxyphenyl)-1*H*-indazole-1-carboxylate. To a solution of compound 9 (1 eq, 100 mg) in 1, 4-dioxane (5 mL) was added DIPEA (3 eq, 96 mg) and acryloyl chloride (2.5 eq, 62 mg) at 0 °C. The reaction solution was stirred at room temperature for 2 h. The mixture was poured into water and extracted with CH_2Cl_2 (3 × 20 mL). The organic layer was washed with saturated aqueous NaCl, dried over anhydrous Na_2SO_4, and concentrated in vacuo to get the crude product. ^{1}H NMR (400 MHz, DMSO-d_6) δ 11.43 (s, 1H), 10.77 (s, 1H), 8.31 (s, 1H), 8.13 (d, J = 8.2 Hz, 1H), 8.00 (d, J = 8.4 Hz, 1H), 7.93 (d, J = 7.5 Hz, 1H), 7.67 (d, J = 8.5 Hz, 1H), 7.59 (t, J = 7.7 Hz,

1H), 7.28 (t, J = 7.5 Hz, 1H), 6.86 (d, J = 1.9 Hz, 2H), 6.58 (s, 1H), 6.39 (dd, J = 17.0, 10.2 Hz, 1H), 6.22 (d, J = 16.9 Hz, 1H), 5.75 (d, J = 10.2 Hz, 1H), 3.83 (s, 6H), 1.67 (s, 9H).

2-acrylamido-*N*-(6-(3,5-dimethoxyphenyl)-1*H*-indazol-3-yl) benzamide (10). To a solution of crude product in the step above in DCM (4 mL) was added TFA (2 mL), the mixture was stirred at room temperature for 2 h. Then the solution was concentrated with a rotary evaporator, extracted with saturated aqueous $NaHCO_3$ and DCM, The organic layer was collected and dried. Then the residue was washed by 2 mL DCM twice to get purity target product 10 (F-1) as a white compound (43 mg, 47%). White powder, 54.5% yield. HPLC analysis: purity = 95.1980%, retention time = 13.058 min ^{1}H NMR (400 MHz, DMSO-d_6): δ 12.91 (s, 1H), 11.11 (s, 1H), 11.02 (s, 1H), 8.34 (d, J = 8.3 Hz, 1H), 8.01 (d, J = 7.7 Hz, 1H), 7.84 (d, J = 8.5 Hz, 1H), 7.70 (s, 1H), 7.60 (t, J = 7.8 Hz, 1H), 7.41 (dd, J = 8.6, 1.2 Hz, 1H), 7.28 (t, J = 7.6 Hz, 1H), 6.86 (d, J = 2.2 Hz, 2H), 6.54 (t, J = 2.1 Hz, 1H), 6.39 (dd, J = 17.0, 10.2 Hz, 1H), 6.24 (dd, J = 17.0, 1.5 Hz, 1H), 5.78 (dd, J = 10.2, 1.5 Hz, 1H), 3.83 (s, 6H). ^{13}C NMR (126 MHz, DMSO-d_6) δ 167.50, 163.27, 160.86, 142.74, 141.60, 139.55, 138.71, 138.45, 132.41, 132.20, 129.09, 127.02, 123.36, 122.34, 122.16, 121.59, 119.74, 116.48, 107.95, 105.35, 99.50, 55.30. HRMS (ACPI) *m/z* calcd. for $C_{25}H_{22}N_4O_4$ $[M + H]^+$: 443.1714. Found: 443.1715.

4.2.1. 2-Acrylamido-N-(6-(3-methoxyphenyl)-1H-indazol-3-yl) benzamide (F-2)

White powder, 47.5% yield. HPLC analysis: purity = 96.3415%, retention time = 13.108 min ^{1}H NMR (400 MHz, DMSO-d_6): δ 12.93 (s, 1H), 11.10 (s, 1H), 11.03 (s, 1H), 8.32 (d, J = 8.0 Hz, 1H), 8.01 (d, J = 7.3 Hz, 1H), 7.85 (d, J = 8.4 Hz, 1H), 7.69 (s, 1H), 7.59 (t, J = 8.0 Hz, 1H), 7.48−7.36 (m, 2H), 7.23−7.34 (m 3H), 6.97 (d, J = 8.0 Hz, 1H), 6.39 (dd, J = 16.9, 10.1 Hz, 1H), 6.23 (d, J = 16.9 Hz, 1H), 5.77 (d, J = 10.8 Hz, 1H), 3.85 (s, 3H). ^{13}C NMR (126 MHz, DMSO-d_6): δ 167.53, 163.28, 159.76, 142.05, 141.68, 139.57, 138.66, 138.47, 132.42, 132.20, 129.98, 129.10, 127.01, 123.36, 122.33, 122.24, 121.60, 119.71, 119.51, 116.41, 113.14, 112.68, 107.88, 55.16. HRMS (ACPI) *m/z* calcd. for $C_{24}H_{20}N_4O_3$ $[M + H]^+$: 413.1608. Found: 413.1607.

4.2.2. 2-Acrylamido-N-(6-(4-methoxyphenyl)-1H-indazol-3-yl) benzamide (F-3)

White powder, 46.3% yield. HPLC analysis: purity = 98.7086%, retention time = 12.818 min ^{1}H NMR (400 MHz, DMSO-d_6): δ 12.93 (s, 1H), 11.10 (s, 1H), 11.03 (s, 1H), 8.32 (d, J = 8.0 Hz, 1H), 8.01 (d, J = 7.3 Hz, 1H), 7.85 (d, J = 8.4 Hz, 1H), 7.69 (s, 1H), 7.59 (t, J = 8.0 Hz, 1H), 7.48−7.36 (m, 2H), 7.23−7.34 (m 3H), 6.97 (d, J = 8.0 Hz, 1H), 6.39 (dd, J = 16.9, 10.1 Hz, 1H), 6.23 (d, J = 16.9 Hz, 1H), 5.77 (d, J = 10.8 Hz, 1H), 3.85 (s, 3H). ^{13}C NMR (126 MHz, DMSO-d_6): δ 167.51, 163.28, 158.99, 141.87, 139.71, 138.54, 138.39, 132.84, 132.49, 132.08, 129.12, 128.19, 126.95, 123.29, 122.39, 122.18, 121.52, 119.34, 115.87, 114.41, 106.95, 55.19. HRMS (ACPI) *m/z* calcd. for $C_{24}H_{20}N_4O_3$ $[M + H]^+$: 413.1608. Found: 413.1609.

4.2.3. 2-Acrylamido-N-(6-(3,5-dimethylphenyl)-1H-indazol-3-yl) benzamide (F-4)

White powder, 47.2% yield. HPLC analysis: purity = 99.1762%, retention time = 13.886 min ^{1}H NMR (400 MHz, DMSO-d_6): δ 12.93 (s, 1H), 11.10 (s, 1H), 11.03 (s, 1H), 8.32 (d, J = 8.0 Hz, 1H), 8.01 (d, J = 7.3 Hz, 1H), 7.85 (d, J = 8.4 Hz, 1H), 7.69 (s, 1H), 7.59 (t, J = 8.0 Hz, 1H), 7.48−7.36 (m, 2H), 7.23−7.34 (m 3H), 6.97 (d, J = 8.0 Hz, 1H), 6.39 (dd, J = 16.9, 10.1 Hz, 1H), 6.23 (d, J = 16.9 Hz, 1H), 5.77 (d, J = 10.8 Hz, 1H), 3.85 (s, 3H). ^{13}C NMR (126 MHz, DMSO-d_6): δ 167.53, 163.27, 141.75, 140.43, 139.54, 139.00, 138.47, 137.91, 132.42, 132.19, 129.10, 128.91, 127.00, 124.96, 123.35, 122.32, 122.12, 121.58, 119.68, 116.26, 107.58, 20.98. HRMS (ACPI) *m/z* calcd. for $C_{25}H_{22}N_4O_2$ $[M + H]^+$: 411.1816. Found: 411.1814.

4.2.4. 2-Acrylamido-N-(6-(2-methoxypyridin-4-yl)-1H-indazol-3-yl)benzamide (F-5)

White powder, 56.8% yield. HPLC analysis: purity = 98.1307%, retention time = 12.679 min ^{1}H NMR (500 MHz, DMSO-d_6): δ 13.07 (s, 1H), 11.10 (s, 1H), 11.06 (s, 1H), 8.33 (d, J = 8.2 Hz, 1H), 8.25 (d, J = 5.3 Hz, 1H), 8.02 (d, J = 7.4 Hz, 1H), 7.91 (d, J = 8.5 Hz, 1H), 7.85 (s, 1H), 7.59 (t, J = 7.7 Hz, 1H), 7.49 (d, J = 8.5 Hz, 1H), 7.39 (d, J = 5.2 Hz, 1H), 7.28 (t, J = 7.5 Hz, 1H), 7.19 (s, 1H), 6.40 (dd, J = 17.0, 10.2 Hz, 1H), 6.24 (d, J = 16.9 Hz, 1H), 5.77 (d, J = 10.3 Hz, 1H). ^{13}C NMR (126 MHz, DMSO-d_6): δ 167.52, 164.45, 163.28, 150.69, 147.42, 141.43, 139.68, 138.41, 135.59, 132.39, 132.19, 129.11, 127.01, 123.38, 122.65, 122.44, 121.65, 119.08, 117.27, 115.56, 108.52, 107.95, 53.22. HRMS (ACPI) *m/z* calcd. for $C_{23}H_{19}N_5O_3$ $[M + H]^+$: 414.1561. Found: 414.1568.

4.2.5. 2-Acrylamido-N-(6-(thiophen-2-yl)-1H-indazol-3-yl) benzamide (F-6)

White powder, 61.2% yield. HPLC analysis: purity = 96.4612%, retention time = 12.863 min ^{1}H NMR (400 MHz, DMSO-d_6): δ 12.90 (s, 1H), 11.07 (s, 1H), 11.02 (s, 1H), 8.31 (d, J = 8.3 Hz, 1H), 7.99 (d, J = 7.5 Hz, 1H), 7.82 (d, J = 8.5 Hz, 1H), 7.69 (s, 1H), 7.65−7.54 (m, 3H), 7.43 (dd, J = 8.6, 1.2 Hz, 1H), 7.27 (t, J = 7.5 Hz, 1H), 7.17 (dd, J = 5.0, 3.7 Hz, 1H), 6.39 (dd, J = 17.0, 10.2 Hz, 1H), 6.23 (dd, J = 17.0, 1.5 Hz, 1H), 5.77 (dd, J = 10.2, 1.4 Hz, 1H). ^{13}C NMR (126 MHz, DMSO-d_6): δ 167.48, 163.28, 143.60, 141.53, 139.75, 138.40, 132.41, 132.19, 132.07, 129.09, 128.55, 127.02, 125.84, 124.24, 123.37, 122.63, 122.43, 121.63, 118.54, 116.32, 106.11. HRMS (ACPI) *m/z* calcd. for $C_{21}H_{16}N_4O_2S$ $[M + H]^+$: 389.1067. Found: 389.1069.

4.2.6. 2-Acrylamido-N-(6-(thiophen-3-yl)-1H-indazol-3-yl) benzamide (F-7)

White powder, 51.7% yield. HPLC analysis: purity = 96.5045%, retention time = 12.763 min ^{1}H NMR (500 MHz, DMSO-d_6): δ 12.88 (s, 1H), 11.09 (s, 1H), 10.99 (s, 1H), 8.33 (d, J = 8.1 Hz, 1H), 8.00 (d, J = 7.1 Hz, 1H), 7.97 (s, 1H), 7.80 (d, J = 8.5 Hz, 1H), 7.75 (s, 1H), 7.71−7.63 (m, 2H), 7.59 (t, J = 7.6 Hz, 1H), 7.49 (d, J = 8.5 Hz, 1H), 7.28 (t, J = 7.4 Hz, 1H), 6.39 (dd, J = 17.0, 10.2 Hz, 1H), 6.23 (d, J = 17.0 Hz, 1H), 5.78 (d, J = 10.3 Hz, 1H). ^{13}C NMR (126 MHz, DMSO-d_6): δ 167.49, 163.28, 141.72, 141.61, 139.61, 138.44, 133.53, 132.42, 132.19, 129.09, 127.08, 127.02, 126.48, 123.36, 122.38, 122.22, 121.60, 121.48, 119.22, 116.09, 106.84. HRMS (ACPI) *m/z* calcd. For $C_{21}H_{16}N_4O_2S$ $[M + H]^+$: 389.1067. Found: 389.1067.

4.2.7. 2-Acrylamido-N-(6-(2,3-dihydrobenzofuran-5-yl)-1H-indazol-3-yl)benzamide (F-8)

White powder, 52.4% yield. HPLC analysis: purity = 97.9621%, retention time = 12.746 min ^{1}H NMR (400 MHz, DMSO-d_6): δ 13.02 (s, 1H), 11.09 (s, 2H), 8.32 (d, J = 8.1 Hz, 1H), 8.03 (d, J = 7.3 Hz, 1H), 7.80 (d, J = 8.5 Hz, 1H), 7.66−7.51 (m, 3H), 7.45 (d, J = 8.3 Hz, 1H), 7.32 (d, J = 8.4 Hz, 1H), 7.26 (t, J = 7.2 Hz, 1H), 6.86 (d, J = 8.3 Hz, 1H), 6.41 (dd, J = 17.0, 10.0 Hz, 1H), 6.23 (d, J = 16.6 Hz, 1H), 5.77 (d, J = 6.1 Hz, 1H), 4.58 (t, J = 8.7 Hz, 2H), 3.25 (t, J = 8.6 Hz, 2H). ^{13}C NMR (126 MHz, DMSO-d_6): δ 167.49, 163.30, 159.50, 141.87, 139.70, 138.90, 138.52, 133.04, 132.53, 132.03, 129.19, 128.19, 126.86, 123.89, 123.28, 122.66, 122.04, 121.55, 119.39, 115.79, 109.16, 106.95, 71.18, 29.09. HRMS (ACPI) *m/z* calcd. for $C_{25}H_{20}N_4O_3$ $[M + H]^+$: 425.1608. Found: 425.1608.

4.2.8. 2-Acrylamido-N-(6-(3-(trifluoromethoxy)phenyl)-1H-indazol-3-yl)benzamide (F-9)

White powder, 48.1% yield. HPLC analysis: purity = 96.4298%, retention time = 12.856 min ^{1}H NMR (400 MHz, DMSO-d_6): δ 13.03 (s, 1H), 11.11 (s, 1H), 11.07 (s, 1H), 8.33 (d, J = 8.2 Hz, 1H), 8.02 (d, J = 7.6 Hz, 1H), 7.90 (d, J = 8.5 Hz, 1H), 7.81 (d, J = 7.8 Hz, 1H), 7.77 (s, 1H), 7.74 (s, 1H), 7.68−7.55 (m, 2H), 7.45 (d, J = 8.5 Hz, 1H), 7.40 (d,

J = 8.1 Hz, 1H), 7.28 (t, J = 7.5 Hz, 1H), 6.40 (dd, J = 17.0, 10.2 Hz, 1H), 6.24 (d, J = 16.8 Hz, 1H), 5.77 (d, J = 11.9 Hz, 1H). ^{13}C NMR (126 MHz, DMSO-d_6): δ 167.54, 163.28, 148.98, 142.91, 141.59, 139.64, 138.44, 136.92, 132.41, 132.18, 130.84, 129.11, 126.98, 126.28, 123.36, 123.22, 122.56, 122.40, 121.62, 121.18, 119.75, 119.65, 119.46, 119.14, 117.10, 116.71, 108.33. HRMS (ACPI) *m/z* calcd. for $C_{24}H_{17}F_3N_4O_3$ $[M + H]^+$: 467.1325. Found: 467.1324.

4.2.9. 2-Acrylamido-N-(6-(2-fluoro-5-(trifluoromethoxy)phenyl)-1H-indazol-3-yl)benzamide (F-10)

White powder, 46.5% yield. HPLC analysis: purity = 98.8326%, retention time = 13.480 min ^{1}H NMR (500 MHz, DMSO-d_6): δ 13.05 (s, 1H), 11.11 (s, 1H), 11.07 (s, 1H), 8.34 (d, J = 8.2 Hz, 1H), 8.03 (d, J = 7.6 Hz, 1H), 7.91 (d, J = 8.5 Hz, 1H), 7.70 (s, 1H), 7.66 (dd, J = 6.0, 2.3 Hz, 1H), 7.59 (t, J = 7.8 Hz, 1H), 7.55–7.40 (m, 2H), 7.35–7.20 (m, 2H), 6.40 (dd, J = 17.0, 10.2 Hz, 1H), 6.24 (dd, J = 17.0, 1.2 Hz, 1H), 5.77 (dd, J = 10.3, 1.1 Hz, 1H). ^{13}C NMR (126 MHz, DMSO-d_6): δ 167.57, 163.28, 158.53, 156.57, 144.54, 141.07, 139.68, 138.43, 132.40, 132.20, 131.65, 130.34, 130.21, 129.11, 126.98, 123.76, 123.73, 123.37, 123.14, 122.40, 122.19, 122.15, 121.63, 121.10, 120.88, 120.87, 119.06, 118.02, 117.81, 117.02, 116.70, 110.68. HRMS (ACPI) *m/z* calcd. for $C_{24}H_{16}F_4N_4O_3$ $[M + H]^+$: 485.1231. Found: 485.1232.

4.2.10. 2-Acrylamido-N-(6-(2-fluoro-3-methoxyphenyl)-1H-indazol-3-yl)benzamide (F-11)

White powder, 51.5% yield. HPLC analysis: purity = 98.8745%, retention time = 12.749 min ^{1}H NMR (400 MHz, DMSO-d_6): δ 12.98 (s, 1H), 11.10 (s, 1H), 11.06 (s, 1H), 8.33 (d, J = 8.3 Hz, 1H), 8.01 (d, J = 7.6 Hz, 1H), 7.86 (d, J = 8.5 Hz, 1H), 7.67–7.54 (m, 2H), 7.35–7.17 (m, 4H), 7.14 (dd, J = 9.6, 4.5 Hz, 1H), 6.40 (dd, J = 17.0, 10.1 Hz, 1H), 6.24 (d, J = 15.9 Hz, 1H), 5.77 (d, J = 11.2 Hz, 1H), 3.89 (s, 3H). ^{13}C NMR (126 MHz, DMSO-d_6): δ 167.55, 163.28, 149.80, 147.86, 147.85, 147.78, 141.17, 139.62, 138.44, 133.18, 132.41, 132.20, 129.26, 129.18, 129.10, 127.01, 124.53, 124.50, 123.37, 122.37, 121.92, 121.62, 121.17, 121.16, 116.40, 113.06, 110.27, 110.25, 56.15. HRMS (ACPI) *m/z* calcd. for $C_{24}H_{19}FN_4O_3$ $[M + H]^+$: 431.1514. Found: 431.1513.

4.2.11. 2-Acrylamido-N-(6-(4-fluoro-3-methoxyphenyl)-1H-indazol-3-yl)benzamide (F-12)

White powder, 53.3% yield. HPLC analysis: purity = 99.0780%, retention time = 12.805 min ^{1}H NMR (500 MHz, DMSO-d_6): δ 12.93 (s, 1H), 11.11 (s, 1H), 11.03 (s, 1H), 8.34 (d, J = 6.9 Hz, 1H), 8.02 (d, J = 5.5 Hz, 1H), 7.86 (dd, J = 8.4, 2.4 Hz, 1H), 7.71 (s, 1H), 7.59 (t, J = 7.7 Hz, 1H), 7.48 (d, J = 7.8 Hz, 1H), 7.42 (d, J = 8.5 Hz, 1H), 7.36–7.08 (m, 3H), 6.39 (dd, J = 17.0, 10.2 Hz, 1H), 6.24 (dd, J = 17.0, 1.3 Hz, 1H), 5.78 (dd, J = 10.2, 1.3 Hz, 1H), 3.97 (s, 3H). ^{13}C NMR (126 MHz, DMSO-d_6): δ 167.51, 163.27, 152.34, 150.39, 147.41, 147.32, 141.64, 139.60, 138.45, 138.02, 137.56, 137.53, 132.42, 132.18, 129.10, 127.00, 123.36, 122.38, 122.24, 121.60, 119.72, 119.51, 119.46, 116.31, 116.21, 116.06, 112.87, 107.93, 56.11. HRMS (ACPI) *m/z* calcd. for $C_{24}H_{19}FN_4O_3$ $[M + H]^+$: 431.1514. Found: 431.1505.

4.2.12. 2-Acrylamido-N-(6-(3-fluoro-5-methoxyphenyl)-1H-indazol-3-yl)benzamide (F-13)

White powder, 39.8% yield. HPLC analysis: purity = 97.7365%, retention time = 13.105 min ^{1}H NMR (400 MHz, DMSO-d_6): δ 12.99 (s, 1H), 11.10 (s, 1H), 11.06 (s, 1H), 8.33 (d, J = 8.2 Hz, 1H), 8.01 (d, J = 7.7 Hz, 1H), 7.87 (d, J = 8.5 Hz, 1H), 7.75 (s, 1H), 7.60 (t, J = 7.7 Hz, 1H), 7.43 (d, J = 9.1 Hz, 1H), 7.28 (t, J = 7.5 Hz, 1H), 7.18 (d, J = 9.8 Hz, 1H), 7.15 (s, 1H), 6.87 (dd, J = 10.9, 1.9 Hz, 1H), 6.40 (dd, J = 17.0, 10.1 Hz, 1H), 6.24 (dd, J = 17.0, 1.1 Hz, 1H), 5.78 (dd, J = 10.3, 1.1 Hz, 1H), 3.87 (s, 3H). ^{13}C NMR (126 MHz, DMSO-d_6): δ 167.51, 164.34, 163.28, 162.42, 161.11, 161.01, 143.48, 143.39, 141.52, 139.60, 138.43, 137.39, 132.40, 132.19, 129.10, 127.01, 123.37, 122.36, 121.63, 119.54, 116.70, 109.16, 108.20, 106.21, 106.03, 100.67, 100.47, 55.74. HRMS (ACPI) *m/z* calcd. for $C_{24}H_{19}FN_4O_3$ $[M + H]^+$: 431.1514. Found: 431.1512.

4.2.13. 2-Acrylamido-N-(6-(2-fluoro-5-methoxyphenyl)-1H-indazol-3-yl)benzamide (F-14)

White powder, 44.4% yield. HPLC analysis: purity = 98.4778%, retention time = 12.955 min ^{1}H NMR (400 MHz, DMSO-d_6): δ 12.96 (s, 1H), 11.10 (s, 1H), 11.03 (s, 1H), 8.33 (d, J = 8.2 Hz, 1H), 8.02 (d, J = 7.8 Hz, 1H), 7.86 (d, J = 8.5 Hz, 1H), 7.64 (s, 1H), 7.59 (t, J = 7.8 Hz, 1H), 7.27 (dd, J = 11.1, 8.3 Hz, 3H), 7.12 (dd, J = 6.4, 3.1 Hz, 1H), 6.94–7.02 (m, 1H), 6.39 (dd, J = 17.0, 10.2 Hz, 1H), 6.23 (dd, J = 17.0, 1.5 Hz, 1H), 5.77 (dd, J = 10.2, 1.5 Hz, 1H), 3.81 (s, 3H). ^{13}C NMR (126 MHz, DMSO-d_6): δ 167.54, 163.28, 155.69, 154.44, 152.55, 141.17, 139.61, 138.44, 133.29, 132.41, 132.21, 129.10, 128.99, 127.02, 123.38, 122.37, 121.91, 121.62, 121.13, 116.88, 116.69, 116.41, 115.59, 115.56, 114.54, 114.47, 110.31, 110.29, 55.71. HRMS (ACPI) *m/z* calcd. for $C_{24}H_{19}FN_4O_3$ $[M + H]^+$: 431.1514. Found: 431.1512.

4.2.14. 2-Acrylamido-N-(6-(3,5-dimethoxyphenyl)-1H-pyrazolo[3,4-b]pyridin-3-yl)benzamide (F-15)

White powder, 45.6% yield. HPLC analysis: purity = 97.4189%, retention time = 13.061 min ^{1}H NMR (400 MHz, DMSO-d_6): δ 13.17 (s, 1H), 10.81 (s, 2H), 8.42 (d, J = 8.5 Hz, 1H), 8.20 (d, J = 8.1 Hz, 1H), 7.96 (d, J = 7.5 Hz, 1H), 7.79 (d, J = 8.6 Hz, 1H), 7.57 (t, J = 7.6 Hz, 1H), 7.32 (d, J = 2.0 Hz, 2H), 7.31–7.16 (m, 1H), 6.62 (s, 1H), 6.44 (dd, J = 17.0, 10.2 Hz, 1H), 6.23 (d, J = 16.9 Hz, 1H), 5.76 (d, J = 11.2 Hz, 1H), 3.84 (s, 6H). ^{13}C NMR (126 MHz, DMSO-d_6): δ 167.18, 163.33, 160.82, 155.45, 151.99, 140.81, 139.22, 138.01, 133.02, 132.36, 131.97, 129.20, 126.95, 123.50, 123.44, 121.95, 113.80, 107.89, 105.16, 101.57, 55.39. HRMS (ACPI) *m/z* calcd. for $C_{24}H_{21}N_5O_4$ $[M + H]^+$: 444.1666. Found: 444.1665.

4.2.15. 2-Acrylamido-N-(6-(3-methoxyphenyl)-1H-pyrazolo[3,4-b]pyridin-3yl)benzamide (F-16)

White powder, 54.3% yield. HPLC analysis: purity = 96.8679%, retention time = 12.939 min ^{1}H NMR (400 MHz, DMSO-d_6): δ 13.46 (s, 1H), 11.24 (s, 1H), 10.94 (s, 1H), 8.45 (d, J = 8.5 Hz, 1H), 8.25 (d, J = 8.2 Hz, 1H), 7.97 (d, J = 7.6 Hz, 1H), 7.80 (d, J = 8.6 Hz, 1H), 7.75 (d, J = 7.4 Hz, 2H), 7.59 (t, J = 7.7 Hz, 1H), 7.45 (t, J = 7.9 Hz, 1H), 7.28 (t, J = 7.6 Hz, 1H), 7.13–7.01 (m, 1H), 6.43 (dd, J = 17.0, 10.2 Hz, 1H), 6.25 (d, J = 16.1 Hz, 1H), 5.84–5.71 (m, 1H), 3.86 (s, 3H). ^{13}C NMR (126 MHz, DMSO-d_6): δ 172.43, 168.54, 164.98, 160.86, 157.34, 145.40, 144.39, 143.36, 138.42, 137.59, 137.35, 135.13, 134.46, 132.29, 128.73, 128.29, 127.09, 124.82, 120.54, 119.00, 117.48, 113.02, 60.45. HRMS (ACPI) *m/z* calcd. for $C_{23}H_{19}N_5O_3$ $[M + H]^+$: 414.1561. Found: 444.1560.

4.2.16. 2-Acrylamido-N-(6-(4-fluoro-3-methoxyphenyl)-1H-pyrazolo[3,4-b]pyridin-3yl)benzamide (F-17)

White powder, 44.8% yield. HPLC analysis: purity = 95.4518%, retention time = 12.558 min ^{1}H NMR (400 MHz, DMSO-d_6): δ 13.45 (s, 1H), 11.22 (s, 1H), 10.93 (s, 1H), 8.44 (d, J = 8.5 Hz, 1H), 8.24 (d, J = 8.2 Hz, 1H), 7.95 (dd, J = 11.5, 4.7 Hz, 2H), 7.83 (d, J = 8.6 Hz, 1H), 7.79–7.72 (m, 1H), 7.58 (t, J = 7.8 Hz, 1H), 7.36 (dd, J = 11.1, 8.6 Hz, 1H), 7.28 (t, J = 7.5 Hz, 1H), 6.43 (dd, J = 17.0, 10.2 Hz, 1H), 6.24 (dd, J = 17.0, 1.1 Hz, 1H), 5.77 (d, J = 11.4 Hz, 1H), 3.98 (s, 3H). ^{13}C NMR (126 MHz, DMSO-d_6): δ 167.17, 163.28, 154.84, 153.56, 152.03, 151.59, 147.45, 147.36, 139.16, 138.08, 135.59, 135.56, 133.19, 132.34, 132.08, 129.16, 127.00, 123.47, 123.08, 121.90, 119.96, 119.91, 116.19, 116.05, 113.57, 112.39, 107.66, 56.07. HRMS (ACPI) *m/z* calcd. for $C_{23}H_{18}FN_5O_3$ $[M + H]^+$: 432.1466. Found: 432.1467.

4.2.17. 2-Acrylamido-N-(6-(3-fluoro-5-methoxyphenyl)-1H-pyrazolo[3,4-b]pyridin-3yl)benzamide (F-18)

White powder, 51.1% yield. HPLC analysis: purity = 96.3863%,

retention time = 12.702 min ^{1}H NMR (500 MHz, DMSO-d_6): δ 13.44 (s, 1H), 11.17 (s, 2H), 8.47 (d, J = 8.5 Hz, 1H), 8.25 (d, J = 8.2 Hz, 1H), 7.97 (d, J = 7.6 Hz, 1H), 7.83 (d, J = 8.6 Hz, 1H), 7.65−7.52 (m, 3H), 7.27 (t, J = 7.5 Hz, 1H), 6.95 (d, J = 10.7 Hz, 1H), 6.43 (dd, J = 17.0, 10.2 Hz, 1H), 6.25 (d, J = 17.0 Hz, 1H), 5.84−5.71 (m, 1H), 3.88 (s, 3H). ^{13}C NMR (126 MHz, DMSO-d_6): δ 167.20, 164.34, 163.29, 162.42, 161.11, 161.02, 154.20, 154.18, 151.94, 141.58, 141.50, 139.32, 138.11, 133.34, 132.36, 132.04, 129.19, 126.97, 123.43, 123.14, 121.87, 113.72, 108.89, 108.14, 106.08, 105.89, 102.62, 102.42, 55.79. HRMS (ACPI) m/z calcd. for $C_{23}H_{18}FN_5O_3$ [M + H]$^+$: 432.1466. Found: 432.1466.

4.2.18. 2-Acrylamido-N-(6-(2-fluoro-5-methoxyphenyl)-1H-pyrazolo[3,4-b]pyridin3yl)benzamide (F-19)

White powder, 53.9% yield. HPLC analysis: purity = 96.8993%, retention time = 13.085 min ^{1}H NMR (400 MHz, DMSO-d_6): δ 13.54 (s, 1H), 11.26 (s, 1H), 10.92 (s, 1H), 8.46 (d, J = 8.5 Hz, 1H), 8.23 (d, J = 8.0 Hz, 1H), 7.96 (d, J = 7.6 Hz, 1H), 7.59 (dd, J = 10.1, 4.0 Hz, 2H), 7.46 (dd, J = 6.1, 3.2 Hz, 1H), 7.36−7.23 (m, 2H), 7.13−7.03 (m, 1H), 6.43 (dd, J = 17.0, 10.2 Hz, 1H), 6.24 (d, J = 15.8 Hz, 1H), 5.77 (d, J = 11.0 Hz, 1H), 3.83 (s, 3H). ^{13}C NMR (126 MHz, DMSO-d_6): δ 167.23, 163.28, 155.62, 155.28, 153.36, 152.25, 152.23, 151.86, 139.18, 138.11, 132.83, 132.35, 132.12, 129.17, 127.68, 127.57, 127.03, 123.47, 123.00, 121.87, 117.34, 117.14, 116.95, 116.89, 116.61, 116.54, 114.95, 114.93, 107.74, 55.73. HRMS (ACPI) m/z calcd. for $C_{23}H_{18}FN_5O_3$ [M + H]$^+$: 432.1466. Found: 432.1464.

4.2.19. N-(6-(3,5-dimethoxyphenyl)-1H-indazol-3-yl)-2-propionamidobenzamide (F-20)

White powder, 62.2% yield. HPLC analysis: purity = 98.3956%, retention time = 12.982 min ^{1}H NMR (400 MHz, DMSO-d_6): δ 12.93 (s, 1H), 11.01 (s, 1H), 10.88 (s, 1H), 8.33 (d, J = 8.4 Hz, 1H), 7.99 (d, J = 8.0 Hz, 1H), 7.83 (d, J = 8.5 Hz, 1H), 7.70 (s, 1H), 7.56 (t, J = 7.5 Hz, 1H), 7.41 (dd, J = 8.6, 0.6 Hz, 1H), 7.23 (t, J = 7.7 Hz, 1H), 6.86 (d, J = 2.1 Hz, 2H), 6.54 (t, J = 1.9 Hz, 1H), 3.83 (s, 6H), 2.36 (q, J = 7.5 Hz, 2H), 1.08 (t, J = 7.5 Hz, 3H). ^{13}C NMR (126 MHz, DMSO-d_6): δ 171.81, 167.62, 160.87, 142.75, 141.63, 139.59, 138.94, 138.74, 132.21, 129.04, 122.74, 122.12, 121.54, 121.14, 119.75, 116.48, 107.98, 105.36, 99.50, 55.29, 30.30, 9.39. HRMS (ACPI) m/z calcd. for $C_{25}H_{24}N_4O_4$ [M + H]$^+$: 445.1870. Found: 445.1867.

4.2.20. 2-(2-chloroacetamido)-N-(6-(3,5-dimethoxyphenyl)-1H-indazol-3-yl)benzamide (F-21)

White powder, 59.7% yield. HPLC analysis: purity = 96.4727%, retention time = 12.933 min ^{1}H NMR (400 MHz, DMSO-d_6): δ 12.97 (s, 1H), 11.54 (s, 1H), 11.13 (s, 1H), 8.40 (d, J = 8.3 Hz, 1H), 8.05 (d, J = 7.3 Hz, 1H), 7.83 (d, J = 8.5 Hz, 1H), 7.72 (s, 1H), 7.62 (t, J = 7.7 Hz, 1H), 7.42 (d, J = 8.6 Hz, 1H), 7.31 (t, J = 7.5 Hz, 1H), 6.87 (d, J = 2.0 Hz, 2H), 6.54 (s, 1H), 4.42 (s, 2H), 3.83 (s, 6H). ^{13}C NMR (126 MHz, DMSO-d_6): δ 167.35, 165.00, 160.86, 142.72, 141.63, 139.45, 138.78, 137.95, 132.38, 129.14, 123.65, 122.10, 121.84, 121.02, 119.80, 116.43, 108.02, 105.37, 99.53, 55.31, 43.38. HRMS (ACPI) m/z calcd. for $C_{24}H_{21}ClN_4O_4$ [M + H]$^+$: 465.1324. Found: 465.1320.

4.2.21. N-(6-(3,5-dimethoxyphenyl)-1H-indazol-3-yl)-2-(3-methylbut-2enamido) benzamide (F-22)

White powder, 60.7% yield. HPLC analysis: purity = 98.5531%, retention time = 13.613 min ^{1}H NMR (400 MHz, DMSO-d_6): δ 12.93 (s, 1H), 11.01 (s, 1H), 10.90 (s, 1H), 8.40 (d, J = 8.3 Hz, 1H), 8.01 (d, J = 7.7 Hz, 1H), 7.82 (d, J = 8.5 Hz, 1H), 7.71 (s, 1H), 7.56 (t, J = 7.8 Hz, 1H), 7.41 (dd, J = 8.6, 1.1 Hz, 1H), 7.22 (t, J = 7.5 Hz, 1H), 6.86 (d, J = 2.2 Hz, 2H), 6.54 (t, J = 2.1 Hz, 1H), 5.79 (s, 1H), 3.83 (s, 6H), 2.14 (s, 3H), 1.84 (s, 3H). ^{13}C NMR (126 MHz, DMSO-d_6): δ 167.77, 164.38, 160.87, 152.51, 142.74, 141.61, 139.55, 139.23, 138.73, 132.22, 129.04, 122.63, 122.05, 121.20, 120.98, 119.76, 119.29, 116.51, 107.98, 105.37, 99.48, 55.30, 26.76, 19.58. HRMS (ACPI) m/z calcd. for $C_{27}H_{26}N_4O_4$ [M + H]$^+$: 471.2027. Found: 471.2027.

4.2.22. N-(6-(3,5-dimethoxyphenyl)-1H-indazol-3-yl)-2-methacrylamidobenzamide (F-23)

White powder, 59.6% yield. HPLC analysis: purity = 96.3535%, retention time = 13.463 min ^{1}H NMR (400 MHz, DMSO-d_6): δ 12.98 (s, 1H), 11.67 (s, 1H), 11.13 (s, 1H), 8.56 (d, J = 8.3 Hz, 1H), 8.11 (d, J = 7.7 Hz, 1H), 7.79 (d, J = 8.5 Hz, 1H), 7.72 (s, 1H), 7.62 (t, J = 7.8 Hz, 1H), 7.42 (d, J = 9.2 Hz, 1H), 7.26 (t, J = 7.7 Hz, 1H), 6.87 (d, J = 2.0 Hz, 2H), 6.54 (s, 1H), 5.86 (s, 1H), 5.54 (s, 1H), 3.83 (s, 7H), 1.98 (s, 3H). ^{13}C NMR (126 MHz, DMSO-d_6): δ 168.02, 165.60, 160.86, 142.71, 141.63, 140.27, 139.39, 139.34, 138.79, 132.66, 129.19, 122.87, 121.83, 120.83, 120.54, 120.28, 119.91, 116.56, 108.07, 105.36, 99.54, 55.30, 18.15. HRMS (ACPI) m/z calcd. for $C_{26}H_{24}N_4O_4$ [M + H]$^+$: 457.1870. Found: 457.1867.

4.2.23. N-(6-(3,5-dimethoxyphenyl)-1H-indazol-3-yl)-2-isobutyramidobenzamide (F-24)

White powder, 58.7% yield. HPLC analysis: purity = 99.0815%, retention time = 13.267 min ^{1}H NMR (400 MHz, DMSO-d_6): δ 12.95 (s, 1H), 11.02 (s, 2H), 8.36 (d, J = 8.3 Hz, 1H), 8.02 (d, J = 7.7 Hz, 1H), 7.83 (d, J = 8.5 Hz, 1H), 7.72 (s, 1H), 7.57 (t, J = 7.7 Hz, 1H), 7.42 (d, J = 8.5 Hz, 1H), 7.23 (t, J = 7.5 Hz, 1H), 6.87 (d, J = 1.6 Hz, 2H), 6.54 (s, 1H), 3.83 (s, 6H), 2.55 (dd, J = 13.8, 6.9 Hz, 1H), 1.13 (d, J = 6.9 Hz, 6H). ^{13}C NMR (126 MHz, DMSO-d_6): δ 174.84, 167.70, 160.86, 142.74, 141.63, 139.54, 139.11, 138.75, 132.28, 129.06, 122.75, 122.05, 121.35, 121.07, 119.77, 116.50, 108.01, 105.36, 99.53, 55.30, 36.01, 19.23. HRMS (ACPI) m/z calcd. for $C_{26}H_{26}N_4O_4$ [M + H]$^+$: 459.2027. Found: 459.2022.

4.2.24. N-(6-(3,5-dimethoxyphenyl)-1H-indazol-3-yl)-2-pivalamidobenzamide (F-25)

White powder, 57.6% yield. HPLC analysis: purity = 98.2992%, retention time = 13.656min. ^{1}H NMR (400 MHz, DMSO-d_6): δ 12.98 (s, 1H), 11.38 (s, 1H), 11.08 (s, 1H), 8.52 (d, J = 8.3 Hz, 1H), 8.07 (d, J = 7.6 Hz, 1H), 7.77 (d, J = 8.5 Hz, 1H), 7.72 (s, 1H), 7.58 (t, J = 7.5 Hz, 1H), 7.42 (d, J = 8.5 Hz, 1H), 7.22 (t, J = 7.5 Hz, 1H), 6.86 (d, J = 2.1 Hz, 2H), 6.54 (t, J = 2.0 Hz, 1H), 3.83 (s, 6H), 1.21 (s, 9H). ^{13}C NMR (126 MHz, DMSO-d_6): δ 176.46, 168.05, 160.86, 142.70, 141.65, 139.75, 139.36, 138.80, 132.58, 129.09, 122.51, 121.77, 120.47, 120.06, 119.90, 116.56, 108.11, 105.36, 99.56, 55.31, 27.19. HRMS (ACPI) m/z calcd. for $C_{27}H_{28}N_4O_4$ [M + H]$^+$: 473.2183. Found: 473.2187.

4.2.25. 2-(2-chloropropanamido)-N-(6-(3,5-dimethoxyphenyl)-1H-indazol-3yl)benzamide (F-26)

White powder, 55.7% yield. HPLC analysis: purity = 98.0673%, retention time = 13.196 min ^{1}H NMR (400 MHz, DMSO-d_6): δ 12.96 (s, 1H), 11.51 (s, 1H), 11.11 (s, 1H), 8.34 (d, J = 8.4 Hz, 1H), 8.05 (d, J = 7.5 Hz, 1H), 7.84 (d, J = 8.5 Hz, 1H), 7.71 (s, 1H), 7.62 (t, J = 7.8 Hz, 1H), 7.41 (d, J = 8.6 Hz, 1H), 7.31 (t, J = 7.5 Hz, 1H), 6.87 (d, J = 1.5 Hz, 2H), 6.54 (d, J = 1.5 Hz, 1H), 4.82 (q, J = 6.7 Hz, 1H), 3.83 (s, 7H), 1.65 (d, J = 6.8 Hz, 3H). ^{13}C NMR (126 MHz, DMSO-d_6): δ 167.74, 167.35, 160.86, 142.72, 141.62, 139.45, 138.78, 137.99, 132.36, 129.16, 123.70, 122.12, 121.16, 119.78, 116.43, 108.02, 105.36, 99.52, 55.66, 55.30, 21.65. HRMS (ACPI) m/z calcd. for $C_{25}H_{23}ClN_4O_4$ [M + H]$^+$: 479.1481. Found: 479.1481.

4.2.26. 2-(cyclopropanecarboxamido)-N-(6-(3,5-dimethoxyphenyl)-1H-indazol-3yl)benzamide (F-27)

White powder, 63.5% yield. HPLC analysis: purity = 98.7522%, retention time = 13.130 min ^{1}H NMR (500 MHz, DMSO-d_6): δ 12.91 (s, 1H), 11.10 (s, 1H), 10.99 (s, 1H), 8.26 (d, J = 8.2 Hz, 1H), 7.99 (d, J = 7.5 Hz, 1H), 7.85 (d, J = 8.5 Hz, 1H), 7.71 (s, 1H), 7.55 (t, J = 7.8 Hz, 1H), 7.42 (dd, J = 8.5, 1.0 Hz, 1H), 7.23 (t, J = 7.5 Hz, 1H), 6.87 (d, J = 2.1 Hz, 2H), 6.54 (t, J = 2.0 Hz, 1H), 3.83 (s, 6H), 1.79−1.58 (m,

1H), 0.94–0.67 (m, 4H). ^{13}C NMR (126 MHz, DMSO-d_6): δ 171.58, 167.58, 160.86, 142.74, 141.60, 139.60, 138.73, 138.71, 132.15, 129.01, 122.82, 122.20, 121.85, 121.83, 119.71, 116.46, 107.95, 105.35, 99.49, 55.30, 15.51, 7.41. HRMS (ACPI) *m/z* calcd. for $C_{26}H_{24}N_4O_4$ $[M + H]^+$: 457.1870. Found: 457.1874.

4.2.27. 3-Acrylamido-N-(6-(3,5-dimethoxyphenyl)-1H-indazol-3-yl)benzamide (F-28)

White powder, 57.4% yield. HPLC analysis: purity = 98.9477%, retention time = 12.561 min ^{1}H NMR (400 MHz, DMSO-d_6): δ 12.95 (s, 1H), 10.85 (s, 1H), 10.61 (s, 1H), 8.34 (s, 1H), 7.97 (d, J = 7.9 Hz, 1H), 7.80 (t, J = 8.0 Hz, 2H), 7.70 (s, 1H), 7.49 (t, J = 7.9 Hz, 1H), 7.39 (d, J = 8.6 Hz, 1H), 6.85 (d, J = 1.8 Hz, 2H), 6.63–6.53 (m, 1H), 6.53 (d, J = 1.9 Hz, 1H), 6.29 (d, J = 17.0 Hz, 1H), 5.78 (d, J = 10.4 Hz, 1H), 3.83 (s, 6H). ^{13}C NMR (126 MHz, DMSO-d_6): δ 165.62, 163.40, 160.85, 142.79, 141.63, 140.08, 139.26, 138.61, 134.63, 131.86, 128.76, 126.94, 122.62, 122.54, 122.17, 119.56, 119.27, 116.44, 107.98, 105.34, 99.49, 55.31. HRMS (ACPI) *m/z* calcd. for $C_{25}H_{22}N_4O_4$ $[M + H]^+$: 443.1714. Found: 443.1708.

4.2.28. N-(6-(3,5-dimethoxyphenyl)-1H-indazol-3-yl)-3-propionamidobenzamide (F-29)

White powder, 56.8% yield. HPLC analysis: purity = 98.9258%, retention time = 12.586 min ^{1}H NMR (500 MHz, DMSO-d_6): δ 12.86 (s, 1H), 10.80 (s, 1H), 10.07 (s, 1H), 8.22 (s, 1H), 7.87 (d, J = 7.9 Hz, 1H), 7.78 (t, J = 8.0 Hz, 2H), 7.69 (s, 1H), 7.46 (t, J = 7.9 Hz, 1H), 7.40 (d, J = 8.6 Hz, 1H), 6.86 (d, J = 1.9 Hz, 2H), 6.54 (s, 1H), 3.83 (s, 6H), 2.36 (q, J = 7.5 Hz, 2H), 1.11 (t, J = 7.5 Hz, 3H). ^{13}C NMR (126 MHz, DMSO-d_6): δ 172.18, 165.65, 160.85, 142.77, 141.62, 140.14, 139.52, 138.65, 135.12, 134.53, 128.68, 122.19, 122.07, 119.59, 118.95, 116.48, 107.95, 105.34, 99.49, 55.30, 29.51, 9.59. HRMS (ACPI) *m/z* calcd. for $C_{25}H_{24}N_4O_4$ $[M + H]^+$: 445.1870. Found: 445.1873.

4.2.29. 3-(2-chloroacetamido)-N-(6-(3,5-dimethoxyphenyl)-1H-indazol-3-yl)benzamide (F-30)

White powder, 61.7% yield. HPLC analysis: purity = 98.4646%, retention time = 12.533 min ^{1}H NMR (400 MHz, DMSO-d_6): δ 12.88 (s, 1H), 10.88 (s, 1H), 10.53 (s, 1H), 8.24 (s, 1H), 7.92–7.82 (m, 2H), 7.79 (d, J = 8.5 Hz, 1H), 7.70 (s, 1H), 7.51 (t, J = 7.9 Hz, 1H), 7.40 (d, J = 8.6 Hz, 1H), 6.86 (d, J = 2.1 Hz, 2H), 6.54 (d, J = 2.0 Hz, 1H), 4.30 (s, 2H), 3.83 (s, 6H). ^{13}C NMR (126 MHz, DMSO-d_6): δ 165.45, 164.87, 160.86, 142.77, 141.64, 140.10, 138.68, 138.63, 134.70, 128.93, 123.04, 122.60, 122.19, 119.61, 119.33, 116.45, 107.96, 105.36, 99.50, 55.30, 43.50. HRMS (ACPI) *m/z* calcd. for $C_{24}H_{21}ClN_4O_4$ $[M + H]^+$: 465.1324. Found: 465.1340.

4.2.30. 3-(2-chloropropanamido)-N-(6-(3,5-dimethoxyphenyl)-1H-indazol-3yl)benzamide (F-31)

White powder, 63.4% yield. HPLC analysis: purity = 99.1385%, retention time = 12.698 min ^{1}H NMR (400 MHz, DMSO-d_6): δ 12.89 (s, 1H), 10.89 (s, 1H), 10.56 (s, 1H), 8.27 (s, 1H), 7.86 (t, J = 9.6 Hz, 2H), 7.79 (d, J = 8.5 Hz, 1H), 7.70 (s, 1H), 7.52 (t, J = 7.9 Hz, 1H), 7.40 (d, J = 8.6 Hz, 1H), 6.86 (d, J = 2.1 Hz, 2H), 6.54 (t, J = 2.0 Hz, 1H), 4.71 (q, J = 6.6 Hz, 1H), 3.83 (s, 6H), 1.64 (d, J = 6.6 Hz, 3H). ^{13}C NMR (126 MHz, DMSO-d_6): δ 167.52, 165.45, 160.86, 142.77, 141.64, 140.09, 138.67, 138.64, 134.69, 128.92, 123.07, 122.66, 122.19, 119.61, 119.44, 116.45, 107.96, 105.35, 99.49, 55.30, 54.75, 21.00. HRMS (ACPI) *m/z* calcd. for $C_{25}H_{23}ClN_4O_4$ $[M + H]^+$: 479.1480. Found: 479.1488.

4.2.31. N-(6-(3,5-dimethoxyphenyl)-1H-indazol-3-yl)-3-(3-methylbut-2enamido)benzamide (F-32)

White powder, 49.6% yield. HPLC analysis: purity = 99.3849%, retention time = 12.690 min ^{1}H NMR (500 MHz, DMSO-d_6): δ 12.87 (s, 1H), 10.81 (s, 1H), 10.06 (s, 1H), 8.28 (s, 1H), 7.88 (d, J = 8.0 Hz, 1H), 7.79 (d, J = 8.5 Hz, 1H), 7.76 (d, J = 7.7 Hz, 1H), 7.69 (s, 1H), 7.45 (t, J = 7.9 Hz, 1H), 7.40 (d, J = 8.6 Hz, 1H), 6.86 (d, J = 2.1 Hz, 2H), 6.54 (t, J = 1.9 Hz, 1H), 5.91 (s, 1H), 3.83 (s, 6H), 2.18 (s, 3H), 1.88 (s, 3H). ^{13}C NMR (126 MHz, DMSO-d_6): δ 165.70, 164.74, 160.85, 151.74, 142.78, 141.63, 140.16, 139.71, 138.64, 134.52, 128.64, 122.22, 122.02, 119.57, 119.01, 118.94, 116.47, 107.95, 105.33, 99.48, 55.30, 27.03, 19.51. HRMS (ACPI) *m/z* calcd. for $C_{27}H_{26}N_4O_4$ $[M + H]^+$: 471.2027. Found: 471.2025.

4.2.32. N-(6-(3,5-dimethoxyphenyl)-1H-indazol-3-yl)-3-methacrylamidobenzamide (F-33)

White powder, 56.5% yield. HPLC analysis: purity = 99.5540%, retention time = 12.940 min ^{1}H NMR (400 MHz, DMSO-d_6): δ 12.89 (s, 1H), 10.86 (d, J = 9.1 Hz, 1H), 10.01 (s, 1H), 8.34 (s, 1H), 7.97 (dd, J = 8.1, 1.3 Hz, 1H), 7.81 (dd, J = 11.9, 8.3 Hz, 2H), 7.70 (s, 1H), 7.49 (t, J = 7.9 Hz, 1H), 7.41 (dd, J = 8.6, 1.1 Hz, 1H), 6.87 (d, J = 2.2 Hz, 2H), 6.55 (t, J = 2.1 Hz, 1H), 5.88 (s, 1H), 5.56 (s, 1H), 3.84 (s, 6H), 1.98 (s, 3H). ^{13}C NMR (126 MHz, DMSO-d_6): δ 166.85, 165.61, 160.86, 142.78, 141.64, 140.18, 140.15, 139.22, 138.66, 134.41, 128.55, 123.38, 122.64, 122.19, 120.24, 120.22, 119.59, 116.48, 107.95, 105.35, 99.49, 55.30, 18.65. HRMS (ACPI) *m/z* calcd. for $C_{26}H_{24}N_4O_4$ $[M + H]^+$: 457.1870. Found: 457.1872.

4.2.33. 3-(2-chloroacetamido)-N-(6-(2-fluoro-3-methoxyphenyl)-1H-indazol-3yl)benzamide (F1-1)

White powder, 60.7% yield. HPLC analysis: purity = 97.0521%, retention time = 12.351 min ^{1}H NMR (400 MHz, DMSO-d_6): δ 12.93 (s, 1H), 10.90 (s, 1H), 10.53 (s, 1H), 8.24 (s, 1H), 7.85 (d, J = 7.8 Hz, 2H), 7.81 (d, J = 8.5 Hz, 1H), 7.60 (s, 1H), 7.52 (t, J = 7.9 Hz, 1H), 7.28–7.22 (m, 2H), 7.22–7.17 (m, 1H), 7.14 (dd, J = 9.6, 4.5 Hz, 1H), 4.30 (s, 2H), 3.89 (s, 3H). ^{13}C NMR (126 MHz, DMSO-d_6): δ 165.48, 164.86, 149.80, 147.85, 147.78, 141.20, 140.15, 138.64, 134.66, 133.13, 129.27, 129.19, 128.93, 124.53, 124.49, 123.03, 122.60, 121.95, 121.91, 121.04, 119.32, 116.36, 113.06, 110.26, 56.16, 43.51. HRMS (ACPI) *m/z* calcd. for $C_{23}H_{18}ClFN_4O_3$ $[M + H]^+$: 453.1124. Found: 453.1123.

4.2.34. 3-(2-chloroacetamido)-N-(6-(2-fluoro-5-methoxyphenyl)-1H-indazol-3yl)benzamide (F1-2)

White powder, 57.9% yield. HPLC analysis: purity = 98.8851%, retention time = 12.514 min ^{1}H NMR (500 MHz, DMSO-d_6): δ 12.94 (s, 1H), 10.91 (s, 1H), 10.54 (s, 1H), 8.25 (s, 1H), 7.86 (d, J = 6.1 Hz, 2H), 7.82 (d, J = 8.4 Hz, 1H), 7.64 (s, 1H), 7.52 (t, J = 7.7 Hz, 1H), 7.27 (t, J = 9.4 Hz, 2H), 7.12 (d, J = 2.5 Hz, 1H), 6.98 (d, J = 8.6 Hz, 1H), 4.31 (s, 2H), 3.82 (s, 3H). ^{13}C NMR (126 MHz, DMSO-d_6): δ 165.48, 164.87, 155.67, 154.43, 152.54, 141.20, 140.15, 138.64, 134.65, 133.24, 129.12, 129.00, 128.94, 123.03, 122.60, 121.94, 121.02, 119.32, 116.87, 116.68, 116.37, 115.57, 115.55, 114.51, 114.44, 110.31, 110.29, 55.69, 43.51. HRMS (ACPI) *m/z* calcd. for $C_{23}H_{18}ClFN_4O_3$ $[M + H]^+$: 453.1124. Found: 453.1122.

Declaration of competing interest

The authors declare that they have no known competing financial interests or personal relationships that could have appeared to influence the work reported in this paper.

Acknowledgements

This study was supported by the National Natural Science Foundation of China (81473242, 81773579, 21602159, 21877085).

Appendix A. Supplementary data

Supplementary data to this article can be found online at https://doi.org/10.1016/j.ejmech.2021.113219.

References

[1] T. Wenger, D. Miller, K. Evans, FGFR craniosynostosis syndromes overview, in: M.P. Adam, H.H. Ardinger, R.A. Pagon, S.E. Wallace, L.J.H. Bean, K. Stephens, A. Amemiya (Eds.), GeneReviews((R)), Seattle (WA), 1993.

[2] N. Su, M. Jin, L. Chen, Role of FGF/FGFR signaling in skeletal development and homeostasis: learning from mouse models, Bone Res 2 (2014) 14003, https://doi.org/10.1038/boneres.2014.3.

[3] S. Dai, Z. Zhou, Z. Chen, G. Xu, Y. Chen, Fibroblast growth factor receptors (FGFRs): structures and small molecule inhibitors, Cells 8 (6) (2019) 614, https://doi.org/10.3390/cells8060614.

[4] P. Mao, O. Cohen, K.J. Kowalski, J. Kusiel, J.E. Buendia-Buendia, M.S. Cuoco, P. Exman, S.A. Wander, A.G. Waks, U. Nayar, J.H. Chung, S.S. Freeman, O. Rozenblatt-Rosen, V.A. Miller, F. Piccioni, D.E. Root, A. Regev, E.P. Winer, N.U. Lin, N. Wagle, Acquired FGFR and FGF alterations confer resistance to estrogen receptor (ER) targeted therapy in ER+ metastatic breast cancer, Clin. Canc. Res. 26 (22) (2020) 5974–5989, https://doi.org/10.1158/1078-0432.

[5] M.A. Hatlen, O. Schmidt-Kittler, C.A. Sherwin, E. Rozsahegyi, N. Rubin, M.P. Sheets, J.L. Kim, C. Miduturu, N. Bifulco, N. Brooijmans, H. Shi, T. Guzi, A. Boral, C. Lengauer, M. Dorsch, R.D. Kim, Y.K. Kang, B.B. Wolf, K.P. Hoeflich, Acquired on-target clinical resistance validates FGFR4 as a driver of hepatocellular carcinoma, Canc. Discov. 9 (12) (2019) 1686–1695, https://doi.org/10.1158/2159-8290.

[6] X. Lu, H. Chen, A.V. Patterson, J.B. Smaill, K. Ding, Fibroblast growth factor receptor 4 (FGFR4) selective inhibitors as hepatocellular carcinoma therapy: advances and prospects, J. Med. Chem. 62 (6) (2019) 2905–2915, https://doi.org/10.1021/acs.jmedchem.8b01531.

[7] C. Wu, X. Chen, D. Chen, Q. Xia, Z. Liu, F. Li, Y. Yan, Y. Cai, Insight into ponatinib resistance mechanisms in rhabdomyosarcoma caused by the mutations in FGFR4 tyrosine kinase using molecular modeling strategies, Int. J. Biol. Macromol. 135 (2019) 294–302, https://doi.org/10.1016/j.ijbiomac.

[8] J.A. Tucker, T. Klein, J. Breed, A.L. Breeze, R. Overman, C. Phillips, R.A. Norman, Structural insights into FGFR kinase isoform selectivity: diverse binding modes of AZD4547 and ponatinib in complex with FGFR1 and FGFR4, Structure 22 (12) (2014) 1764–1774, https://doi.org/10.1016/j.str.2014.09.019.

[9] F. André, T. Bachelot, M. Campone, F. Dalenc, J.M. Perez-Garcia, S.A. Hurvitz, N. Turner, H. Rugo, J.W. Smith, S. Deudon, M. Shi, Y. Zhang, A. Kay, D.G. Porta, A. Yovine, J. Baselga, Targeting FGFR with dovitinib (TKI258): preclinical and clinical data in breast cancer, Clin. Canc. Res. 19 (13) (2013) 3693–3702, https://doi.org/10.1158/1078-0432.CCR-13-0190.

[10] J.C. Soria, F. DeBraud, R. Bahleda, B. Adamo, F. Andre, R. Dienstmann, A. Delmonte, R. Cereda, J. Isaacson, J. Litten, A. Allen, F. Dubois, C. Saba, R. Robert, M. D'Incalci, M. Zucchetti, M.G. Camboni, J. Tabernero, Phase I/IIa study evaluating the safety, efficacy, pharmacokinetics, and pharmacodynamics of lucitanib in advanced solid tumors, Ann. Oncol. 25 (11) (2014) 2244–2251, https://doi.org/10.1093/annonc/mdu390.

[11] J.M. Gozgit, M.J. Wong, L. Moran, S. Wardwell, Q.K. Mohemmad, N.I. Narasimhan, W.C. Shakespeare, F. Wang, T. Clackson, V.M. Rivera, Ponatinib (AP24534), a multitargeted pan-FGFR inhibitor with activity in multiple FGFR-amplified or mutated cancer models, Mol. Canc. Therapeut. 11 (3) (2012) 690–699, https://doi.org/10.1158/1535-7163.MCT-11-0450.

[12] P.R. Gavine, L. Mooney, E. Kilgour, A.P. Thomas, K. Al-Kadhimi, S. Beck, C. Rooney, T. Coleman, D. Baker, M.J. Mellor, A.N. Brooks, T. Klinowska, AZD4547: an orally bioavailable, potent, and selective inhibitor of the fibroblast growth factor receptor tyrosine kinase family, Canc. Res. 72 (8) (2012) 2045–2056, https://doi.org/10.1158/0008-5472.CAN-11-3034.

[13] V. Guagnano, P. Furet, C. Spanka, V. Bordas, M. Le Douget, C. Stamm, J. Brueggen, M.R. Jensen, C. Schnell, H. Schmid, M. Wartmann, J. Berghausen, P. Drueckes, A. Zimmerlin, D. Bussiere, J. Murray, D. Graus Porta, Discovery of 3-(2,6-dichloro-3,5-dimethoxy-phenyl)-1-{6-[4-(4-ethyl-piperazin-1-yl)-phenylamino]-pyrimidin-4-yl}-1-methyl-urea (NVP-BGJ398), a potent and selective inhibitor of the fibroblast growth factor receptor family of receptor tyrosine kinase, J. Med. Chem. 54 (20) (2011) 7066–7083, https://doi.org/10.1021/jm2006222.

[14] D. Wu, M. Guo, M.A. Philips, L. Qu, L. Jiang, J. Li, X. Chen, Z. Chen, L. Chen, Y. Chen, Crystal structure of the FGFR4/ly2874455 complex reveals insights into the pan-FGFR selectivity of LY2874455, PloS One 11 (9) (2016), e0162491, https://doi.org/10.1371/journal.pone.0162491.

[15] F. Facchinetti, A. Hollebecque, R. Bahleda, Y. Loriot, K.A. Olaussen, C. Massard, L. Friboulet, Facts and new hopes on selective FGFR inhibitors in solid tumors, Clin. Canc. Res. 26 (4) (2020) 764–774, https://doi.org/10.1158/1078-0432.CCR-19-2035.

[16] C.W. Murray, D.R. Newell, P. Angibaud, A successful collaboration between academia, biotech and pharma led to discovery of erdafitinib, a selective FGFR inhibitor recently approved by the FDA, Med. Chem. Commun. 10 (2019) 1509–1511, https://doi.org/10.1039/C9MD90044F.

[17] R. Bahleda, F. Meric-Bernstam, L. Goyal, B. Tran, Y. He, I. Yamamiya, K.A. Benhadji, I. Matos, H.T. Arkenau, Phase 1, first-in-human study of futibatinib, a highly selective, irreversible FGFR1-4 inhibitor in patients with advanced solid tumors, Ann. Oncol. 31 (10) (2020) 1405–1412, https://doi.org/10.1016/j.annonc.2020.06.018.

[18] X. Li, C.P. Guise, R. Taghipouran, Y. Yosaatmadja, A. Ashoorzadeh, W.K. Paik, C.J. Squire, S. Jiang, J. Luo, Y. Xu, Z.C. Tu, X. Lu, X. Ren, A.V. Patterson, J.B. Smaill, K. Ding, 2-Oxo-3, 4-dihydropyrimido[4, 5-d]pyrimidinyl derivatives as new irreversible pan fibroblast growth factor receptor (FGFR) inhibitors, Eur. J. Med. Chem. 135 (2017) 531–543, https://doi.org/10.1016/j.ejmech.2017.04.049.

[19] Z. Huang, L. Tan, H. Wang, Y. Liu, S. Blais, J. Deng, T.A. Neubert, N.S. Gray, X. Li, M. Mohammadi, DFG-out mode of inhibition by an irreversible type-1 inhibitor capable of overcoming gate-keeper mutations in FGF receptors, ACS Chem. Biol. 10 (1) (2015) 299–309, https://doi.org/10.1021/cb500674s.

[20] L. Tan, J. Wang, J. Tanizaki, Z. Huang, A.R. Aref, M. Rusan, S.J. Zhu, Y. Zhang, D. Ercan, R.G. Liao, M. Capelletti, W. Zhou, W. Hur, N. Kim, T. Sim, S. Gaudet, D.A. Barbie, J.R. Yeh, C.H. Yun, P.S. Hammerman, M. Mohammadi, P.A. Janne, N.S. Gray, Development of covalent inhibitors that can overcome resistance to first-generation FGFR kinase inhibitors, Proc. Natl. Acad. Sci. U. S. A. 111 (45) (2014) E4869–E4877, https://doi.org/10.1073/pnas.1403438111.

[21] Y. Wang, L. Li, J. Fan, Y. Dai, A. Jiang, M. Geng, J. Ai, W. Duan, Discovery of potent irreversible pan-fibroblast growth factor receptor (FGFR) inhibitors, J. Med. Chem. 61 (20) (2018) 9085–9104, https://doi.org/10.1021/acs.jmedchem.7b01843.

[22] K.A. Brameld, T.D. Owens, E. Verner, E. Venetsanakos, J.M. Bradshaw, V.T. Phan, D. Tam, K. Leung, J. Shu, J. LaStant, D.G. Loughhead, T. Ton, D.E. Karr, M.E. Gerritsen, D.M. Goldstein, J.O. Funk, Discovery of the irreversible covalent FGFR inhibitor 8-(3-(4-Acryloylpiperazin-1-yl)propyl)-6-(2,6-dichloro-3,5-dimethoxyphenyl)-2-(me thylamino)pyrido[2,3-d]pyrimidin-7(8H)-one (PRN1371) for the treatment of solid tumors, J. Med. Chem. 60 (15) (2017) 6516–6527, https://doi.org/10.1021/acs.jmedchem.7b00360.

[23] M. Hagel, C. Miduturu, M. Sheets, N. Rubin, W. Weng, N. Stransky, N. Bifulco, J.L. Kim, B. Hodous, N. Brooijmans, A. Shutes, C. Winter, C. Lengauer, N.E. Kohl, T. Guzi, First selective small molecule inhibitor of FGFR4 for the treatment of hepatocellular carcinomas with an activated FGFR4 signaling pathway, Canc. Discov. 5 (4) (2015) 424–437, https://doi.org/10.1158/2159-8290.CD-14-1029.

[24] X. Lin, Y. Yosaatmadja, M. Kalyukina, M.J. Middleditch, Z. Zhang, X. Lu, K. Ding, A.V. Patterson, J.B. Smaill, C.J. Squire, Rotational freedom, steric hindrance, and protein dynamics explain BLU554 selectivity for the hinge cysteine of FGFR4, ACS Med. Chem. Lett. 10 (8) (2019) 1180–1186, https://doi.org/10.1021/acsmedchemlett.9b00196.

[25] C. Mo, Z. Zhang, C.P. Guise, X. Li, J. Luo, Z. Tu, Y. Xu, A.V. Patterson, J.B. Smaill, X. Ren, X. Lu, K. Ding, 2-Aminopyrimidine derivatives as new selective fibroblast growth factor receptor 4 (FGFR4) inhibitors, ACS Med. Chem. Lett. 8 (5) (2017) 543–548, https://doi.org/10.1021/acsmedchemlett.7b00091.

[26] Y. Wang, Z. Chen, M. Dai, P. Sun, C. Wang, Y. Gao, H. Zhao, W. Zeng, L. Shen, W. Mao, T. Wang, G. Hu, J. Li, S. Chen, C. Long, X. Chen, J. Liu, Y. Zhang, Discovery and optimization of selective FGFR4 inhibitors via scaffold hopping, Bioorg. Med. Chem. Lett 27 (11) (2017) 2420–2423, https://doi.org/10.1016/j.bmcl.2017.04.014.

[27] J.J. Joshi, H. Coffey, E. Corcoran, J. Tsai, C.L. Huang, K. Ichikawa, S. Prajapati, M.H. Hao, S. Bailey, J. Wu, V. Rimkunas, C. Karr, V. Subramanian, P. Kumar, C. MacKenzie, R. Hurley, T. Satoh, K. Yu, E. Park, N. Rioux, A. Kim, W.G. Lai, L. Yu, P. Zhu, S. Buonamici, N. Larsen, P. Fekkes, J. Wang, M. Warmuth, D.J. Reynolds, P.G. Smith, A. Selvaraj, H3B-6527 is a potent and selective inhibitor of FGFR4 in FGF19-driven hepatocellular carcinoma, Canc. Res. 77 (24) (2017) 6999–7013, https://doi.org/10.1158/0008-5472.CAN-17-1865.

[28] T. Knoepfel, P. Furet, R. Mah, N. Buschmann, C. Leblanc, S. Ripoche, D. Graus-Porta, M. Wartmann, I. Galuba, R.A. Fairhurst, 2-Formylpyridyl ureas as highly selective reversible-covalent inhibitors of fibroblast growth factor receptor 4, ACS Med. Chem. Lett. 9 (3) (2018) 215–220, https://doi.org/10.1021/acsmedchemlett.7b00485.

[29] Z. Zhou, X. Chen, Y. Fu, Y. Zhang, S. Dai, J. Li, L. Chen, G. Xu, Z. Chen, Y. Chen, Characterization of FGF401 as a reversible covalent inhibitor of fibroblast growth factor receptor 4, Chem. Commun. (Camb) 55 (42) (2019) 5890–5893, https://doi.org/10.1039/c9cc02052g.

[30] A. Weiss, F. Adler, A. Buhles, C. Stamm, R.A. Fairhurst, M. Kiffe, D. Sterker, M. Centeleghe, M. Wartmann, J. Kinyamu-Akunda, H.S. Schadt, P. Couttet, A. Wolf, Y. Wang, P. Barzaghi-Rinaudo, M. Murakami, A. Kauffmann, T. Knoepfel, N. Buschmann, C. Leblanc, R. Mah, P. Furet, J. Blank, F. Hofmann, W.R. Sellers, D. Graus Porta, FGF401, A first-in-class highly selective and potent FGFR4 inhibitor for the treatment of FGF19-driven hepatocellular cancer, Mol. Canc. Therapeut. 18 (12) (2019) 2194–2206, https://doi.org/10.1158/1535-7163.MCT-18-1291.

[31] R.A. Norman, A.K. Schott, D.M. Andrews, J. Breed, K.M. Foote, A.P. Garner, D. Ogg, J.P. Orme, J.H. Pink, K. Roberts, D.A. Rudge, A.P. Thomas, A.G. Leach, Protein-ligand crystal structures can guide the design of selective inhibitors of the FGFR tyrosine kinase, J. Med. Chem. 55 (11) (2012) 5003–5012, https://doi.org/10.1021/jm3004043.

[32] W. Yan, X. Wang, Y. Dai, B. Zhao, X. Yang, J. Fan, Y. Gao, F. Meng, Y. Wang, C. Luo, J. Ai, M. Geng, W. Duan, Discovery of 3-(5'-Substituted)-Benzimidazole-5-(1-(3,5-dichloropyridin-4-yl)ethoxy)-1H-indazoles as Potent Fibroblast Growth Factor Receptor Inhibitors: design, Synthesis, and Biological Evaluation, J. Med. Chem. 59 (14) (2016) 6690–6708, https://doi.org/10.1021/acs.jmedchem.6b00056.

[33] C.D. Sohl, M.R. Ryan, B. Luo, K.M. Frey, K.S. Anderson, Illuminating the molecular mechanisms of tyrosine kinase inhibitor resistance for the FGFR1 gatekeeper mutation: the Achilles' heel of targeted therapy, ACS Chem. Biol. 10 (5) (2015) 1319–1329, https://doi.org/10.1021/acschembio.5b00014.

[34] Y. Zafrani, G. Sod-Moriah, D. Yeffet, A. Berliner, D. Amir, D. Marciano, S. Elias, S. Katalan, N. Ashkenazi, M. Madmon, E. Gershonov, S. Saphier, CF2H, a

functional group-dependent hydrogen-bond donor: is it a more or less lipophilic bioisostere of OH, SH, and CH3? J. Med. Chem. 62 (11) (2019) 5628–5637, https://doi.org/10.1021/acs.jmedchem.9b00604.
[35] K. Tomczak, P. Czerwińska, M. Wiznerowicz, The Cancer Genome Atlas (TCGA): an immeasurable source of knowledge, Contemp. Oncol. (Pozn) 19 (1A) (2015) A68–A77, https://doi.org/10.5114/wo.2014.47136.
[36] C. Braicu, M. Buse, C. Busuioc, R. Drula, D. Gulei, L. Raduly, A. Rusu, A. Irimie, A.G. Atanasov, O. Slaby, C. Ionescu, I. Berindan-Neagoe, A comprehensive review on MAPK: a promising therapeutic target in cancer, Cancers (Basel) 11 (10) (2019) 1618, https://doi.org/10.3390/cancers11101618.
[37] Y. Liu, M. Cao, Y. Cai, X. Li, C. Zhao, R. Cui, Dissecting the role of the FGF19-FGFR4 signaling pathway in cancer development and progression, Front Cell Dev Biol 8 (2020) 95, https://doi.org/10.3389/fcell.2020.00095.
[38] B.Y. Lee, P. Timpson, L.G. Horvath, R.J. Daly, FAK signaling in human cancer as a target for therapeutics, Pharmacol. Ther. 146 (2015) 132–149, https://doi.org/10.1016/j.pharmthera.2014.10.001.
[39] A. Fuhrmann, A. Banisadr, P. Beri, T.D. Tlsty, A.J. Engler, Metastatic state of cancer cells may Be indicated by adhesion strength, Biophys. J. 112 (4) (2017) 736–745, https://doi.org/10.1016/j.bpj.2016.12.038.
[40] I. Shimizu, Y. Yoshida, M. Suda, T. Minamino, DNA damage response and metabolic disease, Cell Metabol. 20 (6) (2014) 967–977, https://doi.org/10.1016/j.cmet.2014.10.008.
[41] X. Lin, Y. Yosaatmadja, M. Kalyukina, M.J. Middleditch, Z. Zhang, X. Lu, K. Ding, A.V. Patterson, J.B. Smaill, C.J. Squire, Rotational freedom, steric hindrance, and protein dynamics explain BLU554 selectivity for the hinge cysteine of FGFR4, ACS Med. Chem. Lett. 10 (8) (2019) 1180–1186, https://doi.org/10.1021/acsmedchemlett.9b00196.